Loss of furin in β-cells induces an mTORC1-ATF4 anabolic pathway that leads to β-cell dysfunction

Loss of *Furin* in β cells induces an mTORC1-ATF4 anabolic pathway that leads to β cell dysfunction

Running title: FURIN controls β cell mTORC1 signaling

Bas Brouwers[1,2,#], Ilaria Coppola[1,#], Katlijn Vints[3,4], Bastian Dislich[5,6], Nathalie Jouvet[7], Leentje Van Lommel[8], Charlotte Segers[1,9,10], Natalia V. Gounko[3,4], Lieven Thorrez[11], Frans Schuit[8], Stefan F. Lichtenthaler[5,6,12], Jennifer L. Estall[7], Jeroen Declercq[1,5], Bruno Ramos-Molina[1,13,*] and John W.M. Creemers[1,*]

1 Laboratory for Biochemical Neuroendocrinology, Department of Human Genetics, KU Leuven, Leuven, Belgium; **2** Metabolic Research Laboratories, Wellcome Trust MRC Institute of Metabolic Science, University of Cambridge, Cambridge, UK; **3** VIB-KU Leuven Center for Brain & Disease Research, Electron Microscopy Platform & VIB-Bioimaging Core, Leuven, Belgium; **4** KU Leuven Department of Neurosciences, Leuven Brain Institute, 3000 Leuven, Belgium; **5** German Center for Neurodegenerative Diseases (DZNE), Munich, Germany; **6** Neuroproteomics, School of Medicine, Klinikum rechts der Isar, Technical University of Munich, Munich, Germany; **7** Institut de recherches cliniques de Montréal (IRCM), Montréal, Quebec, Canada; **8** Gene Expression Unit, Department of Cellular and Molecular Medicine, KU Leuven, Leuven, Belgium; **9** Interdisciplinary Biosciences group, Belgian Nuclear Research Centre, SCK CEN, Mol, Belgium; **10** Department of Bioscience Engineering, University of Antwerp, Antwerp, Belgium; **11** Department of Development and Regeneration, KU Leuven campus Kulak, Kortrijk, Belgium; **12** Munich Cluster for Systems Neurology (SyNergy), Munich, Germany; **13** Biomedical Research Institute of Murcia (IMIB-Arrixaca), Murcia, Spain;

***** To whom correspondence should be addressed;

# These authors contributed equally to this manuscript.

Contact information for corresponding authors: mailing address: Laboratory for Biochemical Neuroendocrinology, Department of Human Genetics, KU Leuven, ON I Herestraat 49 – box 607, 3000 Leuven, Belgium; telephone number: +3216379387; fax number: +32 16346073; email addresses: john.creemers@kuleuven.be; brunoramosmolina@gmail.com

Diabetes Publish Ahead of Print, published online December 4, 2020

Abstract

FURIN is a proprotein convertase (PC) responsible for proteolytic activation of a wide array of precursor proteins within the secretory pathway. It maps to the PRC1 locus, a type 2 diabetes susceptibility locus, yet its specific role in pancreatic β cells is largely unknown. The aim of this study was to determine the role of FURIN in glucose homeostasis. We show that *FURIN* is highly expressed in human islets, while PCs that potentially could provide redundancy are expressed at considerably lower levels. β cell-specific *Furin* knockout (β*Fur*KO) mice are glucose intolerant, due to smaller islets with lower insulin content and abnormal dense core secretory granule morphology. mRNA expression analysis and differential proteomics on β*Fur*KO islets revealed activation of Activating Transcription Factor 4 (ATF4), which was mediated by mammalian target of rapamycin C1 (mTORC1). β*Fur*KO cells show impaired cleavage or shedding of the V-ATPase subunits Ac45 and prorenin receptor (PRR), respectively, and impaired lysosomal acidification. Blocking the V-ATPase pharmacologically in β cells increases mTORC1 activity, suggesting the involvement of the V-ATPase proton pump in the phenotype. Taken together, these results suggest a model of mTORC1-ATF4 hyperactivation and impaired lysosomal acidification in β cells lacking *Furin*, which causes β cell dysfunction.

Keywords: FURIN, proprotein convertase, β cell dysfunction, ATF4, mTORC1, Ac45, prorenin receptor.

Many protein hormones are synthesized as large inactive precursors that need proteolytic cleavage to be activated. Proprotein convertases (PCs) are subtilisin-like serine proteases that cleave a variety of precursor proteins in the secretory pathway such as hormones, neuropeptides, extracellular matrix proteins, membrane receptors, and their ligands (1). Any alterations of this regulated process can result in pathological conditions. Typically, when this alteration includes pro-hormones involved in the regulation of glucose and lipid homeostasis, it can result in metabolic disorders (2,3). For instance, PC1/3 and PC2 are both highly expressed in the secretory granules of neuronal and endocrine cells and

process a number of hormones and neuropeptides involved in the regulation of glucose and energy homeostasis such as insulin, glucagon, and proopiomelanocortin (POMC) (2,4). In humans, mutations causing complete loss of PC1/3 enzymatic activity lead to hyperphagic obesity and impaired glucose homeostasis, among other endocrinopathies (4). In addition, common heterozygous PC1/3 mutations that cause partial loss-of-function contribute to variation in human body mass index (BMI) and plasma proinsulin and are associated with impaired regulation of plasma glucose levels (5). On the other hand, genome-wide association studies have found an association between several common variants in the gene encoding human PC2 with diabetes risk and related traits in human populations (6,7).

In contrast, the role of the PCs active in the constitutive secretory pathway, such as FURIN, PC5/6, PACE4, or PC7 in obesity and type 2 diabetes (T2D) has been much less explored. In the secretory pathway, FURIN is active in the *trans*-Golgi network (TGN), endosomes and at the cell membrane. In neuroendocrine cells, FURIN has also been found in immature secretory granules, where it has been proposed to participate in the processing of certain neuropeptides involved in energy metabolism, such as pro-brain-derived neurotrophic factor (BDNF), pro-growth hormone releasing hormone (GHRH), and pro-kisspeptin (KISS1) (8–10). The *FURIN* gene is located near to the *PRC1* T2D association interval and was therefore suggested to be a promising biological T2D candidate (11). In addition, polymorphisms in *FURIN* have been associated with the prevalence of metabolic syndrome (12). We have previously shown that FURIN is crucial for acidification of secretory granules in mouse pancreatic β cells via the cleavage of Ac45, an accessory subunit of the V-ATPase proton pump (13). The V-ATPase complex acidifies intracellular organelles by pumping protons across membranes, and acidification is a critical step in β cell granule maturation and proinsulin-to-insulin conversion by PC1/3 and PC2 (14). However, the significance of protein processing by FURIN in β cell function is incompletely understood.

Recently, we discovered a major artifact in several transgenic mouse lines used in the diabetes field, negatively influencing normal β cell function (15,16). More specifically, we found that human growth hormone (hGH), positioned downstream of the Cre transgene to ensure proper expression, was unexpectedly expressed into a bioactive protein. hGH activates prolactin receptors on β cells, activating a pregnancy-like phenotypic switch. Moreover, pregnancy unrelated changes such as impaired glucose-

stimulated insulin secretion (GSIS) were also observed. This complicates the interpretation of many studies in which these models were used, including our previous FURIN study (13). To unequivocally assess the *in vivo* role of FURIN in β cells, we now generated a conditional knockout mouse model lacking the hGH minigene. Metabolic studies were performed to characterize the function of FURIN in pancreatic β cells *in vivo*. Genomics and proteomics studies and generation of a *Furin* knockout β cell line allowed to determine pathways affected by the absence of FURIN and to identify physiological FURIN substrates that influence β cell function.

Research Design and Methods

Human islets

Human islets from healthy (HbA1c < 6,0) and T2D donors (HbA1c > 6,5 at diagnosis) were obtained from the Alberta Diabetes Institute Islet Core (University of Alberta). **Table S8** contains general information about the donors and additional information is available at https://www.epicore.ualberta.ca/IsletCore/. Islets were cultured overnight until they were handpicked and snap frozen. Protocols were approved by the Human Ethics Committee of IRCM.

Mice

For more details including cell culture, animal procedures, electron microscopy and SILAC methods, please see **Supplemental Material**. RIP-Cre$^{+/-}$ mice were kindly donated by Dr. Pedro L. Herrera (University of Geneva Medical School). *Furin*$^{flox/flox}$ mice were described before (17). Mice were backcrossed at least 8 times to a C57Bl6J background (Janvier). Only male mice were used for experiments throughout the study. All experiments were approved by the KU Leuven Animal Welfare Committee, following the guidelines provided in the Declaration of Helsinki (KU Leuven project number 036/2015).

Microarray analysis

Microarray analysis was performed as described before (15). Briefly, islets were isolated from male Flox and β*Fur*KO mice (12 weeks of age) by collagenase injection in the pancreatic duct. Islet RNA

was isolated using an Absolutely RNA Microprep Kit (Stratagene) according to the manufacturer's protocol. RNA quantity and quality were determined using a Bioanalyser (2100; Agilent). Microarray analysis was performed on MoGene_1.0_ST arrays (Affymetrix). One hundred ng of total islet RNA was hybridized to the arrays according to the manufacturer's manual 701880Rev4. Samples were analyzed pairwise, and $p<0.01$ and fold change ≥ 1.5 were set as selection criteria. Functional enrichment, canonical pathway enrichment and upstream regulator analysis were performed using Ingenuity Pathway Analysis (IPA, Qiagen).

Generation of *Furin* knockout βTC3 cells using the CRISPR-Cas9 nuclease system

The mouse insulinoma cell line βTC3 was cultured in DMEM:F12 (1:1) supplemented with 10% heat inactivated fetal bovine serum, 100 U/ml penicillin, and 100 µg/ml streptomycin. A *Furin* knockout βTC3 cell line was generated using the CRISPR-Cas9 nuclease system, following the protocol as described before (18). Briefly, three 20-nucleotide guide sequences targeting *fur* exon 2 were designed using the online CRISPR Design Tool (http://crispr.mit.edu). The pSpCas9(BB)-2A-Puro construct (Addgene 48139) was used to clone the guide sequences. Optimal transfection and puromycin selection conditions for βTC3 cells were established in advance using a GFP-containing expression construct. To screen guide efficacy, transfected cells were harvested for DNA extraction using the QuickExtract solution, and indel mutations were detected by the SURVEYOR nuclease assay as described. Clonal cells were obtained by serial dilution in 96-well plates (Corning). Genomic microdeletions and insertions were verified by TOPO cloning and subsequent Sanger sequencing. *Furin* deficiency in βTC3 cells was corroborated by western blot using an anti-FURIN antibody. Control cells received the same treatment and were grown in parallel with the knockout lines. Sequences for guide cloning in Addgene vector 48139, and SURVEYOR primer sequences are shown in **Table S9**.

Results

PC expression in human islets of healthy and T2D donors suggests a non-redundant function of FURIN.

To determine the potential importance of FURIN in human islets, we first quantified mRNA expression levels of *Pcsk3* (encoding FURIN) and other PCs in islets from healthy and T2D donors (**Figure 1A)**. Genes encoding PC1/3 and PC2 (*Pcsk1* and *Pcsk2*), which are responsible for processing of proinsulin, proglucagon and prosomatostatin are, as expected, expressed highest. *Pcsk3* showed highest expression of the PCs mainly active in the constitutive secretory and endosomal pathway (PC5/6, PACE4, and PC7, encoded by *Pcsk5*, *Pcsk6* and *Pcsk7*, respectively), consistent with previously published RNAseq datasets from human islets and islet subsets (19,20) (**Figure S1A-B**). Expression levels of these PCs that can potentially provide redundancy for FURIN activity are expressed at much lower levels, which could point to a non-redundant function of FURIN in human β cells. Except for slight increases in *Pcsk5* and *Pcsk6* expression, we did not observe significant changes in PC expression in islets from T2D donors. *INS* expression (encoding INSULIN) was significantly reduced in T2D patients in this cohort (**Figure 1B**). On a protein level, FURIN is expressed at high levels in human β cells and non-β cells (**Figure 1C**). We did not detect differences in control vs. T2D patients, although we are underpowered to make any substantial claims (n=1 per group).

β*Fur*KO mice show elevated blood glucose levels and age-dependent glucose intolerance.

β cell-specific inactivation of *Furin* (β*Fur*KO) was achieved by intercrossing RIP-Cre$^{+/-}$ mice (Tg(Ins2-cre)23Herr] (21) lacking the human growth hormone (hGH) expression enhancer (15,16) with *Furin*-floxed mice (17). As expected, islet *Furin* mRNA (**Figure 2B)** and FURIN protein **(Figure 2C)** expression were strongly reduced. Residual levels are likely caused by expression in islet α and δ cells, and blood vessel endothelial cells, where the Cre transgene is not expressed (21). There was no compensatory increase in expression of PCs that might provide redundancy (**Figure S2A**). Blood glucose levels were mildly but significantly elevated in 10-week-old male β*Fur*KO mice in fed and 6h-fasted states (**Figure S2B**). At this age, male β*Fur*KO mice were significantly glucose intolerant compared to control mice, which worsened as the mice aged **(Figure 2D-F)**. Insulin tolerance tests showed normal peripheral insulin sensitivity **(Figure 2G-I)**, and instead the mice showed severely affected GSIS (**Figure 2J**). Interestingly, no significant differences in glucose tolerance were observed between β*Fur*KO and control females at the age of 10 weeks, indicating that FURIN is not critical for

glucose homeostasis in females at young age (**Figure S2C**). Since glucose homeostasis was unaltered in male flox, Cre and heterozygous mice, nonspecific transgene related effects can be ruled out. Therefore, flox controls were used throughout the rest of the study. It should be noted that Cre expression in this mouse model is not restricted to β cells, but also found in orexigenic RIP-expressing neurons in the hypothalamus (22). However, body weight was not significantly different between β*Fur*KO and control mice on a normal chow diet (**Figure S2D**), suggesting that lack of *Furin* does not have marked effects on body weight regulation by these neurons.

FURIN controls β cell mass, islet insulin content and secretory granule homeostasis

Islets from β*Fur*KO mice appeared smaller than control islets during islet isolations. Indeed, β cell mass and proliferation were significantly reduced in 24-week-old β*Fur*KO mice (**Figure 3A-B**), although islet apoptosis was not different between groups **(Figure 3C)**. Insulin immunoreactivity and pancreatic and islet insulin content were reduced **(Figure 3D-F)**. Ultrastructural analyses showed that *Furin*-deficient β cells were smaller than controls **(Figure 3G-H)**. Despite similar numbers of secretory granules per cell area **(Figure 3I)**, granules in β*Fur*KO islets were smaller, showing reduced halo and core areas **(Figure 3J)**. Furthermore, β cells displayed an increase in the number of immature secretory granules (electron-light core and distinctive halo) **(Figure 3K)**. These results suggest that FURIN is essential for β cell homeostasis and secretory granule biogenesis. *Ex vivo* islet GSIS was unchanged when secreted insulin was adjusted for total islet insulin content (**Figure 3L**) and the ratio (secreted proinsulin)/(secreted insulin) did not differ between genotypes (**Figure 3M**), suggesting that there are no defects in insulin secretion or proinsulin processing in β*Fur*KO islets. Instead, reduced functional β cell mass is likely to be the main driver of the phenotype.

Loss of *Furin* in islet β cells activates an ATF4-dependent anabolic program

To explain the perturbations observed in this model, microarray analysis was performed on β*Fur*KO islets. Although this method does not directly identify FURIN substrates, the notion of differential gene expression might elucidate affected cellular processes, potentially leading to upstream FURIN substrates. We found 126 differentially expressed genes in β*Fur*KO islets (cut-off $p<0.01$ and |fold

change| ≥ 1.5) (**Figure 4A** and **Table S1**). Several mRNAs encoding amino acid (AA) transporters, enzymes involved in AA metabolism and aminoacyl-tRNA synthetases were significantly upregulated **(Figure 4B** and **Table S1)**. Ingenuity Pathway Analysis (IPA) pointed to significant activation of AA metabolism (**Table S2**). The upstream regulator tool predicted activation of Activating Transcription Factor 4 (ATF4, p=2.86E-30) **(Figure 4B** and **Table S3)**, a key transcription factor involved in the integrated stress response (23). Consistently, many stress-induced genes were also upregulated (**Figure 4A-B** and **Table S1**).

Using Stable Isotope Labeling of Amino acids in Cell culture (SILAC), we found 203 differentially expressed proteins in β*Fur*KO islets **(Figure 4C-D and Table S4)** (neg. log p-value cutoff = 2.13682; p=0.0072). Consistent with the microarray data, IPA analysis showed significant changes in AA metabolism **(Table S5)**, and many AA synthesis enzymes showed an increase in expression (**Figure 4C-D**). In addition, canonical pathway analysis predicted activation of 'tRNA charging' (**Table S6**), with 9 aminoacyl-tRNA synthetase proteins being significantly upregulated (**Figure 4C-D** and **Table S4**). Upstream analysis predicted activation of ATF4 (p=3.59E-11) and PKR-like ER kinase (PERK; EIF2AK3, p=3.21E-15)(**Figure 4C-D** and **Table S7**). PERK is an ER-proximal sensor of unfolded proteins that induces ATF4 translation via phosphorylation of Ser51 on eukaryotic initiation factor 2α (eIF2α) (23). These data suggest that β cells lacking *Furin* induce an anabolic program involving upregulation of AA transporters and aminoacyl-tRNA synthetases, likely through activation of the ATF4 transcription factor. Consistent with our data shown in **Figure 3F**, we observed a significant decrease in insulin I by means of SILAC (**Table S4**, ~30% decrease, p=0.01). **Figure S3** shows a good correlation (r=0.4186, p<0.0001) of microarray and SILAC data for all proteins with at least a 25% increase or decrease in expression.

β*Fur*KO islets and β cell lines lacking *Furin* show ATF4 upregulation mediated by mTORC1.

Several kinds of stress conditions increase eIF2α dependent ATF4 translation, with subsequent upregulation of ATF4 target genes (23). Accordingly, we observed significantly increased islet expression of the ATF4 target gene *Trib3* (**Figure 5A**), whereas *Atf4* mRNA levels were unaltered. At

the protein level, both ATF4 and CHOP (another ATF4 target gene) were increased in β*Fur*KO islets, confirming activation of ATF4 (**Figure 5B**). Unexpectedly, β*Fur*KO islets did not exhibit increased phosphorylation of PERK or eIF2α (**Figure 5B**) nor were other ER stress markers increased (**Figure S4A-B**). Emerging evidence suggests that ATF4 translation can also be induced by mammalian target of rapamycin complex 1 (mTORC1) activation (24,25) **(Figure 5C)**. In agreement with this idea, phosphorylation levels of the mTORC1 substrates p70 ribosomal protein S6 kinase (S6K) and eukaryotic translation initiation factor 4E-binding protein 1 (4E-BP1) were augmented in β*Fur*KO islets **(Figure 5D)**. This suggests an activated mTORC1-ATF4 axis in islets from β*Fur*KO mice.

To substantiate our *in vivo* findings in a cellular model, we generated a *Furin* knockout β cell line using the CRISPR-Cas9 system **(Figure S5A-B)**. WST-1 assays demonstrated that cell proliferation and/or viability was significantly reduced in *Furin* knockout βTC3 cells **(Figure 5E)**. In addition, *Furin* knockout βTC3 cells showed increased *Trib3* mRNA **(Figure 5F)** and CHOP and ATF4 protein levels **(Figure 5G)**, suggesting ATF4 activation. Like β*Fur*KO islets, we did not observe increased phosphorylation of eIF2α **(Figure 5G)**, implying that ATF4 upregulation is not mediated by eIF2α. Additionally, *Furin* knockout cells displayed higher mTORC1 activity as demonstrated by the increased phosphorylation levels of S6K **(Figure 5G)**. Treatment with the mTORC1 inhibitor rapamycin reduced ATF4 levels in this cell line, substantiating the idea that mTORC1 activation causes ATF4 upregulation (**Figure 5H**). Together, we conclude that the *Furin* knockout βTC3 cell line can be used as a representative model to investigate the molecular mechanisms caused by *Furin* deficiency in β cells *in vivo*.

Loss of *Furin* in β cells impairs Ac45 processing and PRR shedding, and disrupts lysosomal acidification.

We next sought to determine the mechanism driving mTORC1 hyperactivation in *Fur*KO β cells. We focused on the V-ATPase proton pump, as it serves as part of a docking and activation site for mTORC1 on lysosomes (26). Two critical V-ATPase subunits, ATP6AP1/Ac45 and ATP6AP2/(Pro)-renin receptor (PRR) are known FURIN substrates (13,27) and are highly expressed in β cells in mice and humans (13,20,28). The FURIN cleavage sites of the corresponding precursors were shown to be at the

RVAR^{231} and RKSR^{278} sites respectively (13,27) (**Figure 6A**), while PRR can also be cleaved by SKI-1 at a RTIL^{281} site (29). As such, we hypothesized that impaired Ac45 and/or PRR cleavage would lead to disturbed lysosomal acidification hereby affecting mTORC1 activity in β cells. We first investigated the processing of Ac45 and PRR in β*Fur*KO cells. Mature Ac45 is heavily glycosylated and appears as a broad smear around 60 kDa, but the cleaved form can be detected as a 24-kDa peptide when treated with N-glycosidase F (13) (**Figure 6B**). We observed a complete lack of the 24-kDa form, indicating that Ac45 cleavage does not occur in *Fur*KO β cells (**Figure 6B**). In addition, whereas the intracellular amount of cleaved PRR did not appear to be affected, the soluble secreted form (sPRR) was significantly reduced in the medium of *Fur*KO β cells (**Figure 6C**). To measure V-ATPase function indirectly, we performed ImmunoGold electron microscopy on islets that were incubated with the acidotrophic agent 3-(2,4-dinitroanilino)-3'amino-N-methyldipropylamine (DAMP) (13) and quantified the acidification of lysosomes. We observed a ~57% decrease in the number of gold particles per lysosome, demonstrating impaired acidification of lysosomes in β cells from β*Fur*KO animals (**Figure 6D-E**). Lysosomal size was not different between genotypes (**Figure 6F**). Disrupted lysosomal acidification has been shown to induce mTORC1 signalling in osteoclasts (30). To test this in β cells, WT βTC3 cells were treated with the V-ATPase inhibitor bafilomycin A1. This induced the mTORC1-ATF4 axis, confirming that V-ATPase dysfunction can cause the phenotype **(Figure 6G)**. Knockdown of *Atp6ap1*/*Ac45* showed a significant upregulation of ATF4, but no activation of mTORC1 signaling (**Figure 6H**). No indications for activation of the mTORC1 pathway nor ATF4 were observed after knockdown of *Atp6ap2/Prr* (**Figure 6I)**. Likely, these results reflect the compound nature of the phenotype, whereby loss of FURIN results in impaired cleavage for several substrates, leading to the phenotype. Alternatively, the uncleaved proprotein might lead to additional effects that a genetic knockdown cannot replicate.

Discussion

In this study we have demonstrated that FURIN is essential for β cell function, and that the dysregulation of its activity can affect β cells through the induction of the stress factor ATF4 in a mTORC1-dependent manner (**Figure 7**). The most striking phenotype in β*Fur*KO mice is a strong reduction in functional β

cell mass, which might be below the threshold required to maintain adequate glucose homeostasis, and could directly lead to impaired pulsatile insulin secretion (31). Consistent with our previous study (13), we did not observe impairment of total proinsulin processing in this mouse model. In that study, we have shown that while maturation of the less abundant proinsulin II was impaired, labeling of total insulin did not reveal differences. As the major proinsulin I processing enzyme PCSK1 has a relatively broad pH optimum, the impairment of acidification in the β*Fur*KO model is not sufficient to block insulin processing. Moreover, this is also apparent when the ultrastructure of $CPE^{fat/fat}$ (32) and $Pcsk1^{-/-}$ β cells (33) are compared to our model (**Figure 3G**). In the former two, virtually all granules contain electron-lucent (i.e. grayish) cores, which is not the case in β cells lacking *Furin*. These data suggest that, while total insulin content is strongly decreased in β*Fur*KO β cells, processing is largely unaffected.

Whole-genome expression profiling, proteomics analyses and *in vitro* studies pointed towards activation of the transcription factor ATF4 by mTORC1. Consistent with our data, recent studies in other cell types have shown that ATF4 can be activated by mTORC1 independently of its canonical induction via phosphorylated eIF2α. For instance, ATF4 stimulates the *de novo* purine synthesis pathway and transcriptionally regulates AA transporters, metabolic enzymes and aminoacyl-tRNA synthetases in an mTORC1 dependent manner (24,25). Despite increasing evidence in various other cell lines, the importance of this mTORC1-ATF4 axis in β cells is not explored.

mTORC1 is critical in the regulation of β cell survival and proliferation (34). However, chronic hyperactivation of mTORC1 promotes progressive hyperglycemia and hypoinsulinemia accompanied by a reduction in β cell mass (35), which is likely caused by ER stress and impaired autophagic response that lead to β cell failure (36). Islets isolated from T2D patients exhibit increased mTORC1 activation, and genetic or chemical inhibition of mTORC1-S6K signaling in these islets restores insulin secretion (37), suggesting that hyperactive mTORC1 impairs human β cell function. Therefore, it is highly likely that persistent mTORC1 activity leads to β cell dysfunction in β*Fur*KO mice, which could serve as a new genetic model to study mTORC1 hyperactivity in β cells.

Loss of FURIN activity in β cells potentially affects cleavage of several substrates that contribute to the observed phenotype to different extents. We investigated candidate substrates based on a potential link

with the mTORC1-ATF4 axis, and focused on the V-ATPase accessory subunits Ac45 and PRR. FURIN is known to be critical for V-ATPase function in mice (13) and yeast (38), and interestingly, cryo-EM models of the rat (39) and bovine (40) V-ATPase complex revealed that Ac45 and PRR are present as cleaved forms. Here, we show almost complete lack of Ac45 cleavage, and reduced PRR shedding in *Furin* deficient β cells. Previous work in *Xenopus* intermediate pituitary melanotrope cells has shown that deletion of the endoproteolytic processing site in Ac45 causes it to accumulate in the ER (41). As such, disrupted trafficking of Ac45, and potentially V-ATPase subunits, to the secretory pathway might cause disrupted lysosomal acidification and mTORC1 hyperactivity in β*Fur*KO cells. In this context, osteoclasts in which V-ATPase function is disrupted show increased lysosomal pH, which in turn leads to elevated mTORC1 activity in this cell type (30). Our results suggest that in β cells, mTORC1 activity is dependent on lysosomal pH as well. Alternatively, uncleaved Ac45 might modify β cell mTORC1 activity by relaying amino acid sufficiency from the lysosomal lumen, or alter interactions between V-ATPase and mTORC1 components, as was hypothesized for follicular lymphoma patients carrying *ATP6AP1* mutations (42). Similar to Ac45, PRR is highly expressed in murine and human islets, and its expression is reduced in islets from diabetic donors (28). Interestingly, knockdown of *Atp6ap2/Prr* in a β cell line results in an increase in the percentage of ISGs and reduced granular acidification (28), similar to β cells lacking *Furin* (current study and ref. (13)). Mice lacking PRR in β cells exhibit accumulation of large vacuoles that consume insulin content (43). While we did not observe these structures, it does not rule out a contribution of PRR to the phenotype in β*Fur*KO mice, which might exhibit a milder phenotype as a result of reduced PRR shedding. The exact timing and mechanism of PRR cleavage and shedding is still a matter of debate and might be cell type dependent (27,29). We did not observe significant upregulation of mTORC1 activity upon Ac45 or PRR knockdown, which might reflect the fact that the efficiency of gene knockdown is insufficient to obtain a phenotype or that the cause is multifactorial. The phenocopy obtained with bafilomycin suggests a crucial role for the V-ATPase.

Finally, we did not test the efficiency of Cre-mediated *Furin* recombination in RIPHER neurons (22), so we cannot entirely rule out any phenotypic contribution by hypothalamus-specific *Furin* inactivation.

However, the phenocopy observed in a β cell line generated by CRISPR/Cas9 editing strongly suggests a defect at the level of the β cell.

In conclusion, we describe the importance of the proprotein convertase FURIN in the regulation of β cell mass and function *in vivo*, likely related to its function in regulating the V-ATPase activity. Furthermore, we report that lack of *Furin* results in activation of the stress-induced transcription factor ATF4 mediated by mTORC1. As such, this study sheds light on a novel molecular mechanism for the regulation of β cell function by FURIN and provides evidence that it is an important candidate in the PRC1 susceptibility locus for T2D.

Acknowledgements

We would like to thank Sandra Meulemans, Elisa Cauwelierand Cindy Baldwin for technical assistance..

The microarray data were deposited in the Gene Expression Omnibus (GSE150312).

Funding

This work was supported by the FWO Vlaanderen (grant number G0B0617N) and by the Deutsche Forschungsgemeinschaft (DFG, German Research Foundation) under Germany's Excellence Strategy within the framework of the Munich Cluster for Systems Neurology (EXC 2145 SyNergy– ID 390857198). JLE is a Chercheur-boursier from the FRQS and her research was supported by a grant from the CIHR (PJT-148771). BRM was supported by the Miguel Servet Type I program (CP19/00098) from the Institute of Health Carlos III (ISCIII), and co-financed by the European Regional Development Fund. BB and IC were supported by predoctoral fellowships from the FWO Vlaanderen.

Conflict of Interest Statement

The authors have declared that no conflict of interest exists.

Author Contributions

BB, BRM and JWC designed the research. BB, IC, and BRM performed the majority of *in vivo* and cell culture experiments, with help from CS. BB, KV and IC performed the EM analysis. NJ and JLE

performed the experiments with human islets. BD, SFL and JD performed the proteomics analysis. LVL and FS performed the microarray analysis. BB, LT and JD performed bioinformatics analysis of microarray and proteomics data. BB, IC, BRM and JWC collected and analyzed the data and wrote the manuscript with input from the rest of co-authors. All the authors approved the final version of the manuscript. JWC is the guarantor of this work and, as such, has full access to all the data in the study and takes responsibility for the integrity of the data.

References

1. Seidah NG, Prat A. The biology and therapeutic targeting of the proprotein convertases. Nat Rev Drug Discov. 2012 May;11(5):367–83.

2. Chen Y-C, Taylor AJ, Bruce Verchere C. Islet prohormone processing in health and disease [Internet]. Vol. 20, Diabetes, Obesity and Metabolism. 2018. p. 64–76. Available from: http://dx.doi.org/10.1111/dom.13401

3. Seidah NG, Abifadel M, Prost S, Boileau C, Prat A. The Proprotein Convertases in Hypercholesterolemia and Cardiovascular Diseases: Emphasis on Proprotein Convertase Subtilisin/Kexin 9. Pharmacol Rev. 2017 Jan;69(1):33–52.

4. Stijnen P, Ramos-Molina B, O'Rahilly S, Creemers JWM. PCSK1 Mutations and Human Endocrinopathies: From Obesity to Gastrointestinal Disorders. Endocr Rev. 2016 Aug;37(4):347–71.

5. Creemers JWM, Choquet H, Stijnen P, Vatin V, Pigeyre M, Beckers S, et al. Heterozygous mutations causing partial prohormone convertase 1 deficiency contribute to human obesity. Diabetes. 2012 Feb;61(2):383–90.

6. Winters A, Ramos-Molina B, Jarvela TS, Yerges-Armstrong L, Pollin TI, Lindberg I. Functional analysis of PCSK2 coding variants: A founder effect in the Old Order Amish population. Diabetes Res Clin Pract. 2017 Sep;131:82–90.

7. Leak TS, Keene KL, Langefeld CD, Gallagher CJ, Mychaleckyj JC, Freedman BI, et al. Association of the proprotein convertase subtilisin/kexin-type 2 (PCSK2) gene with type 2 diabetes in an African American population. Mol Genet Metab. 2007 Sep;92(1-2):145–50.

8. Seidah NG, Benjannet S, Pareek S, Chrétien M, Murphy RA. Cellular processing of the neurotrophin precursors of NT3 and BDNF by the mammalian proprotein convertases. FEBS Lett. 1996 Feb 5;379(3):247–50.

9. Dey A, Norrbom C, Zhu X, Stein J, Zhang C, Ueda K, et al. Furin and prohormone convertase 1/3 are major convertases in the processing of mouse pro-growth hormone-releasing hormone. Endocrinology. 2004 Apr;145(4):1961–71.

10. Harihar S, Pounds KM, Iwakuma T, Seidah NG, Welch DR. Furin is the major proprotein convertase required for KISS1-to-Kisspeptin processing. PLoS One. 2014 Jan 13;9(1):e84958.

11. Voight BF, Scott LJ, Steinthorsdottir V, Morris AP, Dina C, Welch RP, et al. Twelve type 2 diabetes susceptibility loci identified through large-scale association analysis. Nat Genet. 2010 Jul;42(7):579–89.

12. Ueyama C, Horibe H, Yamase Y, Fujimaki T, Oguri M, Kato K, et al. Association of FURIN and ZPR1 polymorphisms with metabolic syndrome. Biomed Rep. 2015 Sep;3(5):641–7.

13. Louagie E, Taylor NA, Flamez D, Roebroek AJM, Bright NA, Meulemans S, et al. Role of furin in granular acidification in the endocrine pancreas: identification of the V-ATPase subunit Ac45 as a candidate substrate. Proc Natl Acad Sci U S A. 2008 Aug 26;105(34):12319–24.

14. Hou JC, Min L, Pessin JE. Insulin granule biogenesis, trafficking and exocytosis. Vitam Horm. 2009;80:473–506.

15. Brouwers B, de Faudeur G, Osipovich AB, Goyvaerts L, Lemaire K, Boesmans L, et al. Impaired islet function in commonly used transgenic mouse lines due to human growth hormone minigene expression. Cell Metab. 2014 Dec 2;20(6):979–90.

16. de Faudeur G, Brouwers B, Schuit F, Creemers JWM, Ramos-Molina B. Transgenic Artifacts Caused by Passenger Human Growth Hormone. Trends Endocrinol Metab. 2018 Oct;29(10):670–4.

17. Roebroek AJM, Taylor NA, Louagie E, Pauli I, Smeijers L, Snellinx A, et al. Limited redundancy of the proprotein convertase furin in mouse liver. J Biol Chem. 2004 Dec 17;279(51):53442–50.

18. Ran FA, Hsu PD, Wright J, Agarwala V, Scott DA, Zhang F. Genome engineering using the CRISPR-Cas9 system. Nat Protoc. 2013 Nov;8(11):2281–308.

19. Eizirik DL, Sammeth M, Bouckenooghe T, Bottu G, Sisino G, Igoillo-Esteve M, et al. The human pancreatic islet transcriptome: expression of candidate genes for type 1 diabetes and the impact of pro-inflammatory cytokines. PLoS Genet. 2012 Mar 8;8(3):e1002552.

20. Blodgett DM, Nowosielska A, Afik S, Pechhold S, Cura AJ, Kennedy NJ, et al. Novel Observations From Next-Generation RNA Sequencing of Highly Purified Human Adult and Fetal Islet Cell Subsets. Diabetes. 2015 Sep;64(9):3172–81.

21. Herrera PL. Adult insulin- and glucagon-producing cells differentiate from two independent cell lineages. Development. 2000 Jun;127(11):2317–22.

22. Rother E, Belgardt BF, Tsaousidou E, Hampel B, Waisman A, Myers MG Jr, et al. Acute selective ablation of rat insulin promoter-expressing (RIPHER) neurons defines their orexigenic nature. Proc Natl Acad Sci U S A. 2012 Oct 30;109(44):18132–7.

23. Pakos-Zebrucka K, Koryga I, Mnich K, Ljujic M, Samali A, Gorman AM. The integrated stress response. EMBO Rep. 2016;17(10):1374–95.

24. Ben-Sahra I, Hoxhaj G, Ricoult SJH, Asara JM, Manning BD. mTORC1 induces purine synthesis through control of the mitochondrial tetrahydrofolate cycle. Science. 2016 Feb 12;351(6274):728–33.

25. Park Y, Reyna-Neyra A, Philippe L, Thoreen CC. mTORC1 Balances Cellular Amino Acid Supply with Demand for Protein Synthesis through Post-transcriptional Control of ATF4. Cell Rep. 2017 May 9;19(6):1083–90.

26. Zoncu R, Bar-Peled L, Efeyan A, Wang S, Sancak Y, Sabatini DM. mTORC1 senses lysosomal amino acids through an inside-out mechanism that requires the vacuolar H(+)-ATPase. Science. 2011 Nov 4;334(6056):678–83.

27. Cousin C, Bracquart D, Contrepas A, Corvol P, Muller L, Nguyen G. Soluble form of the (pro)renin receptor generated by intracellular cleavage by furin is secreted in plasma. Hypertension. 2009 Jun;53(6):1077–82.

28. Dai FF, Bhattacharjee A, Liu Y, Batchuluun B, Zhang M, Wang XS, et al. A Novel GLP1 Receptor Interacting Protein ATP6ap2 Regulates Insulin Secretion in Pancreatic Beta Cells [Internet]. Vol. 290, Journal of Biological Chemistry. 2015. p. 25045–61. Available from: http://dx.doi.org/10.1074/jbc.m115.648592

29. Nakagawa T, Suzuki-Nakagawa C, Watanabe A, Asami E, Matsumoto M, Nakano M, et al. Site-1 protease is required for the generation of soluble (pro) renin receptor. J Biochem. 2017;161(4):369–79.

30. Hu Y, Carraro-Lacroix LR, Wang A, Owen C, Bajenova E, Corey PN, et al. Lysosomal pH Plays a Key Role in Regulation of mTOR Activity in Osteoclasts. J Cell Biochem. 2016 Feb;117(2):413–25.

31. Kjems LL, Kirby BM, Welsh EM, Veldhuis JD, Straume M, McIntyre SS, et al. Decrease in beta-cell mass leads to impaired pulsatile insulin secretion, reduced postprandial hepatic insulin clearance, and relative hyperglucagonemia in the minipig. Diabetes. 2001 Sep;50(9):2001–12.

32. Naggert JK, Fricker LD, Varlamov O, Nishina PM, Rouille Y, Steiner DF, et al. Hyperproinsulinaemia in obese fat/fat mice associated with a carboxypeptidase E mutation which reduces enzyme activity. Nat Genet. 1995 Jun;10(2):135–42.

33. Zhu X, Orci L, Carroll R, Norrbom C, Ravazzola M, Steiner DF. Severe block in processing of proinsulin to insulin accompanied by elevation of des-64,65 proinsulin intermediates in islets of mice lacking prohormone convertase 1/3 [Internet]. Vol. 99, Proceedings of the National Academy of Sciences. 2002. p. 10299–304. Available from: http://dx.doi.org/10.1073/pnas.162352799

34. Ardestani A, Lupse B, Kido Y, Leibowitz G, Maedler K. mTORC1 Signaling: A Double-Edged Sword in Diabetic β Cells. Cell Metab. 2018 Feb 6;27(2):314–31.

35. Shigeyama Y, Kobayashi T, Kido Y, Hashimoto N, Asahara S-I, Matsuda T, et al. Biphasic response of pancreatic beta-cell mass to ablation of tuberous sclerosis complex 2 in mice. Mol Cell Biol. 2008 May;28(9):2971–9.

36. Bartolome A, Kimura-Koyanagi M, -I. Asahara S, Guillen C, Inoue H, Teruyama K, et al. Pancreatic -Cell Failure Mediated by mTORC1 Hyperactivity and Autophagic Impairment [Internet]. Vol. 63, Diabetes. 2014. p. 2996–3008. Available from: http://dx.doi.org/10.2337/db13-0970

37. Yuan T, Rafizadeh S, Gorrepati KDD, Lupse B, Oberholzer J, Maedler K, et al. Reciprocal regulation of mTOR complexes in pancreatic islets from humans with type 2 diabetes. Diabetologia. 2017 Apr;60(4):668–78.

38. Oluwatosin YE, Kane PM. Mutations in the yeast KEX2 gene cause a Vma−-like phenotype: a possible role for the Kex2 endoprotease in vacuolar acidification. Mol Cell Biol [Internet]. 1998; Available from: https://mcb.asm.org/content/18/3/1534.short

39. Abbas YM, Wu D, Bueler SA, Robinson CV, Rubinstein JL. Structure of V-ATPase from the mammalian brain. Science. 2020 Mar 13;367(6483):1240–6.

40. Wang R, Long T, Hassan A, Wang J, Sun Y, Xie X-S, et al. Cryo-EM structures of intact V-ATPase from bovine brain. Nat Commun. 2020 Aug 6;11(1):3921.

41. Jansen EJR, van Bakel NHM, Olde Loohuis NFM, Hafmans TGM, Arentsen T, Coenen AJM, et al. Identification of domains within the V-ATPase accessory subunit Ac45 involved in V-ATPase transport and Ca2+-dependent exocytosis. J Biol Chem. 2012 Aug 10;287(33):27537–46.

42. Okosun J, Wolfson RL, Wang J, Araf S, Wilkins L, Castellano BM, et al. Recurrent mTORC1-activating RRAGC mutations in follicular lymphoma. Nat Genet. 2016 Feb;48(2):183–8.

43. Binger KJ, Neukam M, Tattikota SG, Qadri F, Puchkov D, Willmes DM, et al. Atp6ap2 deletion causes extensive vacuolation that consumes the insulin content of pancreatic β cells. Proc Natl Acad Sci U S A. 2019 Oct 1;116(40):19983–8.

Figure legends

Figure 1. *FURIN* is highly expressed in human islets. (A) qRT-PCR analysis of 7 closely related PCs in islets from healthy (n=10) vs. T2D (n=13) human donors. Data are normalized to *PCSK1* expression in healthy islets and *18S* was used as a housekeeping gene. **P<0.01. (B) *INS* gene expression in this cohort, normalized to healthy *PCSK1* expression, **P<0.01. (C) Immunofluorescence of dispersed human islets from healthy or T2D donors (n=1 for each group). FURIN (red) is expressed in insulin-expressing β cells (green) and non-β cells. Scale bars 25 μm.

Figure 2. β*Fur*KO mice show progressive glucose intolerance and impaired GSIS. (A) Schematic of the breeding strategy. Mice in which the essential exon 2 of the *Pcsk3* gene is flanked by loxP sites (*Furin*$^{flox/flox}$) are crossed with RIP-Cre$^{+/-}$ mice (21). The latter mouse model does not have the human growth hormone minigene as expression enhancer, and instead has a rabbit β-globin intron and polyadenylation signal (21). Created with BioRender.com (B) qRT-PCR analysis of *Pcsk3* expression in islets from β*Fur*KO or control (*Furin*$^{flox/flox}$) mice, n=4 per genotype. *P<0.05 determined by unpaired t test with Welch's correction. (C) Western blot for FURIN in βFurKO or control (*Furin*$^{flox/flox}$) mice; GAPDH was used as a loading control. (D-F) Intraperitoneal glucose tolerance tests (IPGTTs) on male β*Fur*KO and control mice at 10 (D; n=6-17 mice/group), 20 (E; n=5-15 mice/group) and 36 (F; n=4-12

mice/group) weeks of age. (G-I) Intraperitoneal insulin tolerance tests (IPITTs) on β*Fur*KO and control males at 10 (G), 20 (H) and 36 (I) weeks of age. (J) Twenty-four-week-old β*Fur*KO and control males were injected with a single bolus of 3mg/g BW D-glucose and insulin levels were measured at indicated time points, n=5-16 per group. (D-J) *P<0.05, **P<0.01, ***P<0.001, determined by 2-way repeated measures ANOVA. All data are presented as mean ± SEM. WT: RIP-Cre$^{-/-}$;*Furin*$^{wt/wt}$; Flox: RIP-Cre$^{-/-}$;*Furin*$^{flox/flox}$; Cre: RIP-Cre$^{+/-}$;*Furin*$^{wt/wt}$; Het: RIP-Cre$^{+/-}$;*Furin*$^{flox/wt}$ and β*Fur*KO: RIP-Cre$^{+/-}$;*Furin*$^{flox/flox}$) mice.

Figure 3. Decreased islet and pancreas insulin content, β cell mass, β cell proliferation, and ultrastructural abnormalities in 24-week-old β*Fur*KO mice. (A) β cell mass quantification expressed in mg (n=3 mice/group). *P<0.05 determined by unpaired Student t-test. (B) Percentage of β cell proliferation as measured by Ki67 staining (n=3 mice/group). ***P<0.001 determined by unpaired Student t-test. (C) Islet apoptosis as measured by nucleosome ELISA; data expressed as fold change compared to control values (n=4 mice/group). (D) Representative micrograph of insulin immunoreactivity in male β*Fur*KO and control mice, scale bar = 25μm. (E) Pancreatic and (F) islet insulin content as measured by insulin ELISA; data are expressed as μg insulin per g pancreas (n=4-5 mice/group) and ng insulin per islet (n=36 samples/group), respectively. **P<0.01,***P<0.001 determined by unpaired Student t-test. (G) Representative electron micrographs of islets from 24-week-old control and β*Fur*KO mice. Scale bar = 5 μm. (H) Quantification of total β cell area (n=15-17 cells/group), ***P<0.001 determined by unpaired Student t-test (I) number of granules per β cell area (sum of dense-core granules and immature granules; n=15-17 cells/group), (J) core, halo or dense-core secretory granule area divided by cytoplasmic area (n=15 cells/group), *P<0.05,***P<0.001 determined by 1-way ANOVA with multiple comparisons and (K) immature secretory granules/dense-core secretory granules (ISG/DCSG) ratio in control and *Furin*knockout β cells (n=8 cells/group). ***P<0.001 determined by unpaired Student t-test. (L) Islet GSIS, quantified as the amount of insulin secreted in the medium corrected for total islet insulin content. G5, 5mM glucose; G20, 20mM glucose and G20 + IBMX. (n=4 mice/group) (M) Ratio of secreted proinsulin/insulin (n=4 mice/group), measured in conditioned medium from islets incubated in 20mM glucose. Data was corrected for total

islet insulin content, and normalized to control (set as 1). All data are represented as mean ± SEM, *P<0.05, **P<0.01, ***P<0.001.

Figure 4. Whole-genome expression and quantitative proteomics analyses on β*Fur*KO islets reveal a significant upregulation of Activating Transcription Factor 4 (ATF4) targets. (A) Volcano plot showing differentially expressed genes in β*Fur*KO vs. control islets (n=4 male mice per group). Negative log p-value = 2 was arbitrarily set as cut-off (dotted line). (B) Ingenuity Pathway Analysis on mRNA expression data predict activation of ATF4 (p=2.86E-30). Many of the genes downstream of ATF4 can be classified in 4 different groups: amino acid (AA) transporters, AA metabolism genes, aminoacyl-tRNA synthetases and stress related genes. A full gene list can be found in **Table S1**. Image created with BioRender.com. (C) Volcano plot showing differentially expressed proteins in β*Fur*KO vs. control islets (n=4 male mice per group), as quantified by SILAC. Negative log p-value was calculated to be 2.13682 after multiple hypothesis correction and was set as a cut-off (dotted line). (D) Ingenuity Pathway Analysis on SILAC data predicts activation of ATF4 (p=3.59E-11), downstream protein targets are classified in the same groups as above. A full protein list can be found in **Table S4**. Image created with BioRender.com.

Figure 5. *Furin* knockout islets and β cell lines exhibit mTORC1 dependent activation of ATF4. (A) qRT-PCR analyses of the mRNA levels of *Atf4* and target genes *Chop* and *Trib3* in whole islet lysates from control and β*Fur*KO mice. ***P<0.001 determined by 1-way ANOVA. (B) Immunoblot analyses and quantification of p-PERK, total PERK, p-eIF2α, total eIF2α, ATF4 and CHOP protein levels in whole islet lysates. P-PERK/PERK, p-eIF2α/eIF2α, ATF4 and CHOP signals were normalized to GAPDH. Data represent the mean of 3 independent experiments. *P<0.05 determined by 1-way ANOVA. (C) Mechanisms that increase ATF4 translation and ATF4 dependent gene expression. Created with BioRender.com. (D) Immunoblot analyses of p-S6K and p-4E-BP1 protein levels in whole islet lysates from control and β*Fur*KO mice. (E) Cell proliferation measured with a WST-1 colorimetric assay in control and *Furin* knockout βTC3 cells. Data, expressed as fold change over control cells, are the mean ± SEM of three independent experiments using three different clones.

***P<0.001 determined by unpaired Student t-test. (F) qRT-PCR analyses of *Atf4*, *Chop* and *Trib3* mRNA levels in whole βTC3 lysates. *P<0.05 determined by 1-way ANOVA. (G) Immunoblot analyses of p-eIF2α, ATF4, CHOP, p-S6K, total S6K, p-4E-BP1 and total 4E-BP1 protein levels in whole βTC3 lysates. Quantification of 3-4 independent experiments is shown on the right. *P<0.05 determined by 1-way ANOVA. (H) Immunoblot analyses of p-S6K, total S6K, and ATF4 protein levels in whole cell lysates from βTC3 cells treated either with vehicle (0.01% DMSO) or 100 nM rapamycin for 16 h. Quantification of 4 independent experiments is shown below. *P<0.05 determined by 1-way ANOVA. For immunoblot analyses GAPDH was used as the loading control. For qRT-PCR analyses the values were normalized to *Gapdh* expression and the data are represented as mean ± SEM, n=3-5 per group.

Figure 6. Loss of *Furin* impairs Ac45 and PRR processing or shedding in βTC3 cells, and disrupts lysosomal acidification in β*Fur*KO islets. (A) Schematic illustration of the V-ATPase proton pump, with Ac45 and PRR protein structures highlighted. FURIN and SKI-1 cleavage sites are indicated by arrows. Indicated residues are for the mouse proteins. SP, signal peptide; L1, luminal domain 1; L2, luminal domain 2; TM, transmembrane domain; C, C-terminal domain; S, soluble domain; L, luminal domain; SKI-1, Subtilisin Kexin Isozyme-1. Image created with BioRender.com. (B) HEK293T and βTC3 (WT and *Fur*KO) cells were transfected with a Flag-tagged Ac45 construct. (Left) Western blot of HEK293T cell lysate before and after N-glycosidase F (N-glyc F) treatment, with the processed form (24 kDa) appearing only after deglycosylation. (Right) Western blot of βTC3 cell lysate, wild type (WT) and *Furin* knockout (*Fur*KO), both treated with N-glyc F (right; βTC3 cells). The indicated positions of proAc45 and Ac45 correspond to the predicted MW of the deglycosylated peptide backbone (46 kDa and 24 kDa respectively, black arrows). (C) Full length (fl) and soluble (s)PRR levels in the lysate (upper panel) and conditioned medium (lower panel) of *Furin* knockout (*Fur*KO) and WT βTC3 cells. Quantifications on the right-hand side show n=3 independent experiments. ***P<0.001 determined by 1-way ANOVA. (D) Immunogold electron microscopy on lysosomes using protein A conjugated to 15 nm of colloidal gold on sections of DAMP incubated islets from control and β*Fur*KO mice. Scale bar = 50 nm. (E) Number of gold particles per lysosome and (F) lysosomal area (μm^2) in control and

β*Fur*KO islets (n=20-21 lysosomes). ***P<0.001 determined by unpaired t test with Welch's correction. (G) Western blot for p-S6K, total S6K, p-4E-BP1, total 4E-BP1, ATF4 in βTC3 cells incubated with the V-ATPase inhibitor bafilomycin A1 (50 nM final concentration) for 24h. GAPDH was used as a loading control. Quantification for 3 independent experiments is included. **P<0.01, ***P<0.001 determined by 2 way ANOVA with Post-Hoc Bonferroni's multiple comparisons test. (H) Western blot analysis of p-4E-BP1/4E-BP1, p-S6K/S6K and ATF4 in βTC3 cells that were subjected to *Atp6ap1*/*Ac45* knockdown by siRNA, quantification of n=4 independent experiments is shown, signals were normalized to GAPDH. (I) Western blot analysis of p-4E-BP1/4E-BP1, p-S6K/S6K and ATF4 in βTC3 cells that were subjected to *Atp6ap2*/*Prr* knockdown by siRNA, including quantification of n=3 independent experiments, signals were normalized to GAPDH. *P<0.05 determined by 2 way ANOVA with Post-Hoc Bonferroni's multiple comparisons test.

Figure 7. Schematic overview of phenotypes in β cells lacking *Furin*. FURIN is a proprotein convertase concentrated in the *trans*-Golgi network (TGN) and cycles through a complex trafficking circuit that involves several TGN/endosomal compartments and the cell surface. In (neuro)endocrine cells, FURIN is also present in insulin-containing immature secretory granules (ISGs) and is removed and returned to the TGN before ISGs mature to dense-core secretory granules (DCSGs). β cells lacking *Furin* (*Fur*KO) show reduced cleavage of Ac45 and PRR, essential subunits of the V-ATPase proton pump, resulting in reduced acidification of intracellular organelles (e.g. lysosomes). *Fur*KO cells induce an expression program that involves amino acid (AA) biosynthesis enzymes and transporters, and stress-related genes. This program is induced by a mammalian target of rapamycin complex 1 (mTORC1) – Activating Transcription Factor 4 (ATF4) axis, in an eIF2α independent manner. *Fur*KO cells show increased ISG/DCSG ratio, are smaller and exhibit reduced insulin content, resulting in impaired glucose tolerance in the whole organism. Image created with BioRender.com.

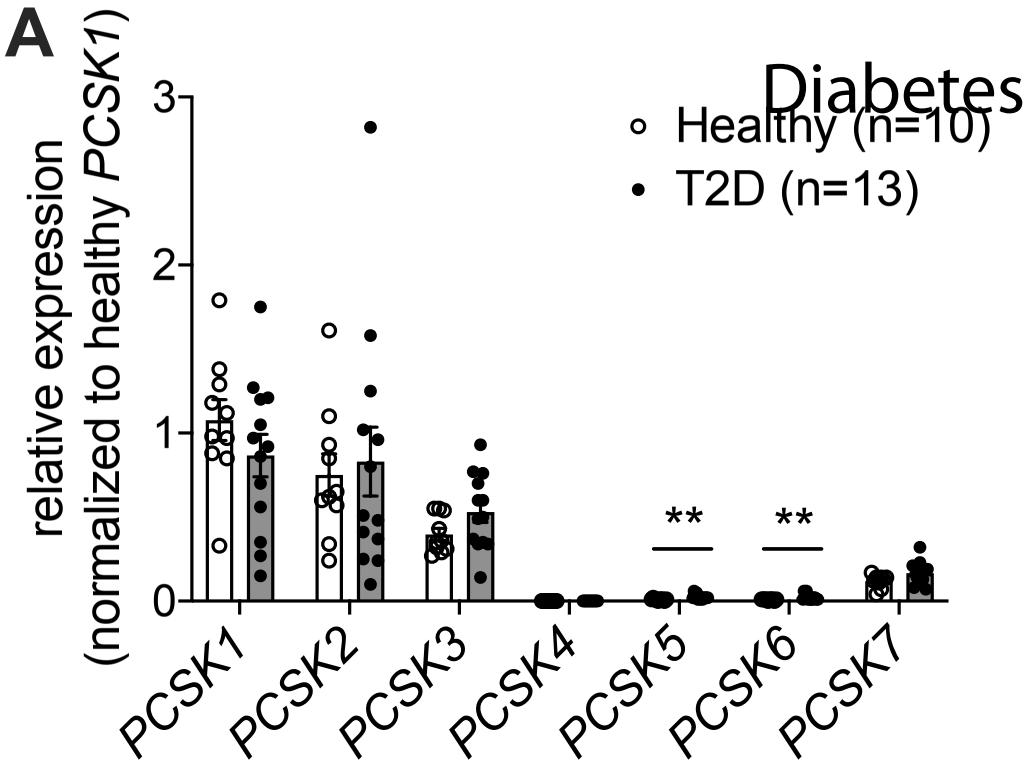
A
relative expression
(normalized to healthy PCSK1)
Healthy (n=10)
T2D (n=13)
0
1
2
3
**
**
PCSK1
PCSK2
PCSK3
PCSK4
PCSK5
PCSK6
PCSK7

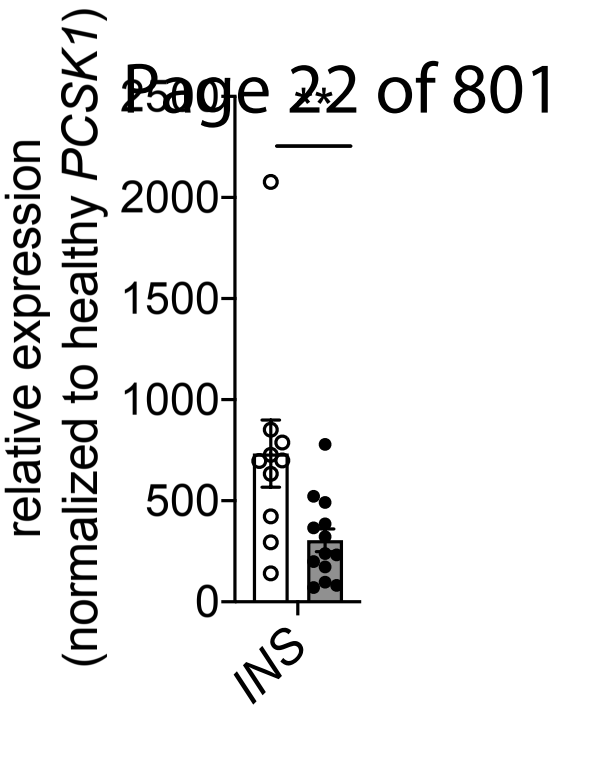
B
relative expression
(normalized to healthy PCSK1)
0
500
1000
1500
2000
2500
**
INS

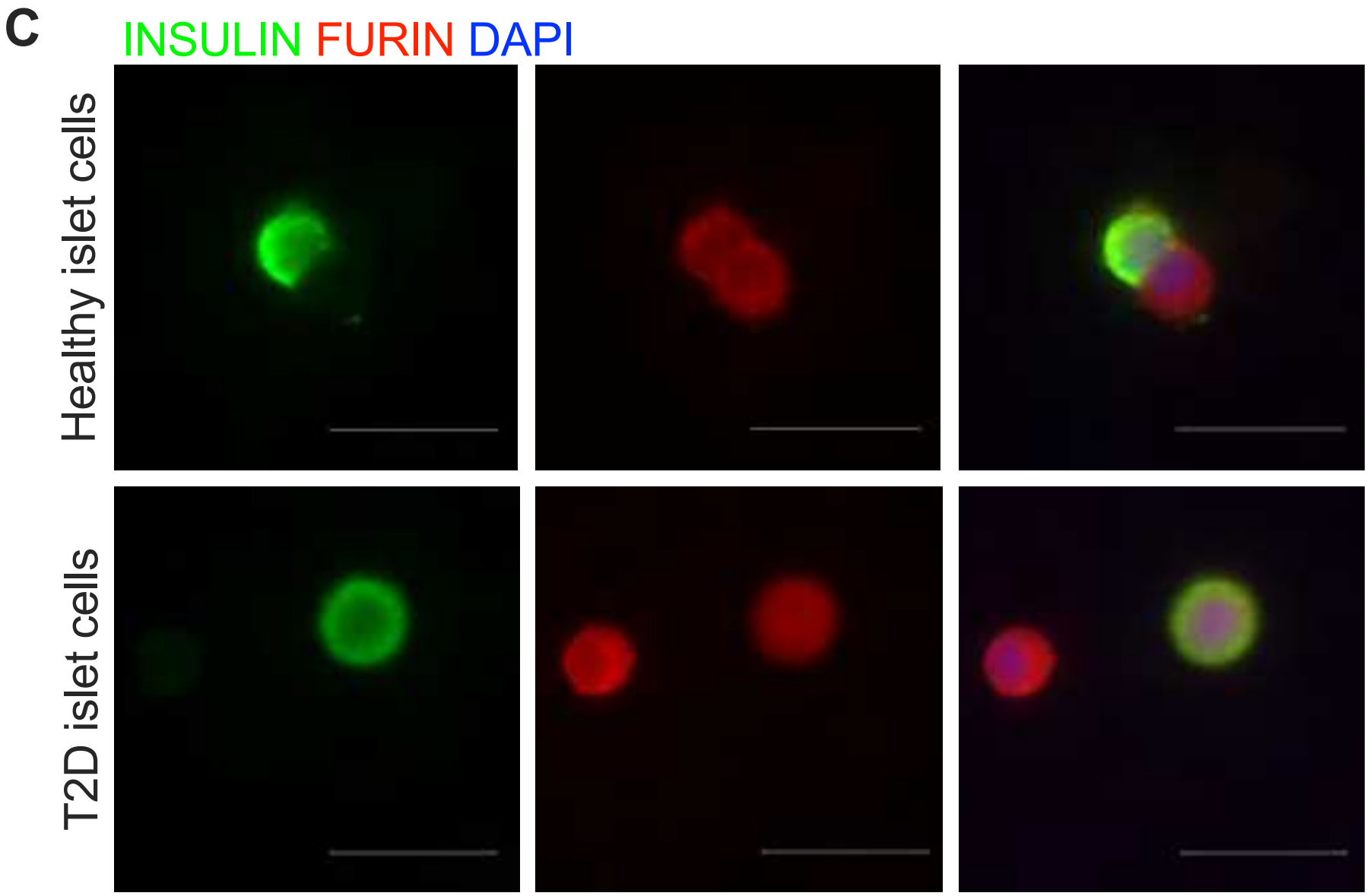
C
INSULIN FURIN DAPI
Healthy islet cells
T2D islet cells

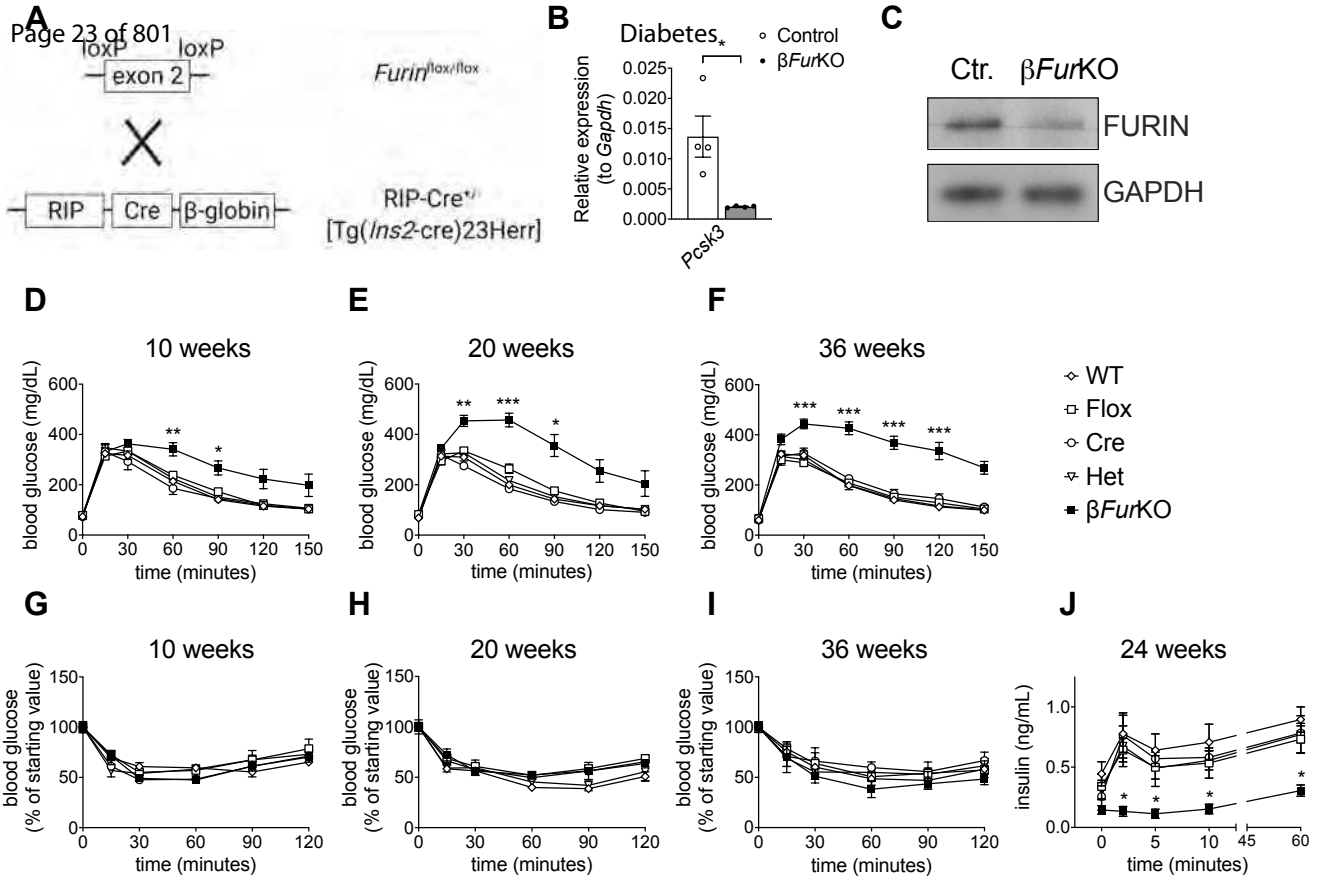
A
loxP
loxP
exon 2
RIP
Cre
β-globin
Furin flox/flox
RIP-Cre +/-
[Tg(Ins2-cre)23Herr]
B
Diabetes*
Control
βFurKO
Relative expression (to Gapdh)
0.025
0.020
0.015
0.010
0.005
0.000
Pcsk3
C
Ctr.
βFurKO
FURIN
GAPDH
D
10 weeks
blood glucose (mg/dL)
time (minutes)
E
20 weeks
F
36 weeks
WT
Flox
Cre
Het
βFurKO
G
10 weeks
blood glucose (% of starting value)
H
20 weeks
I
36 weeks
J
24 weeks
insulin (ng/mL)

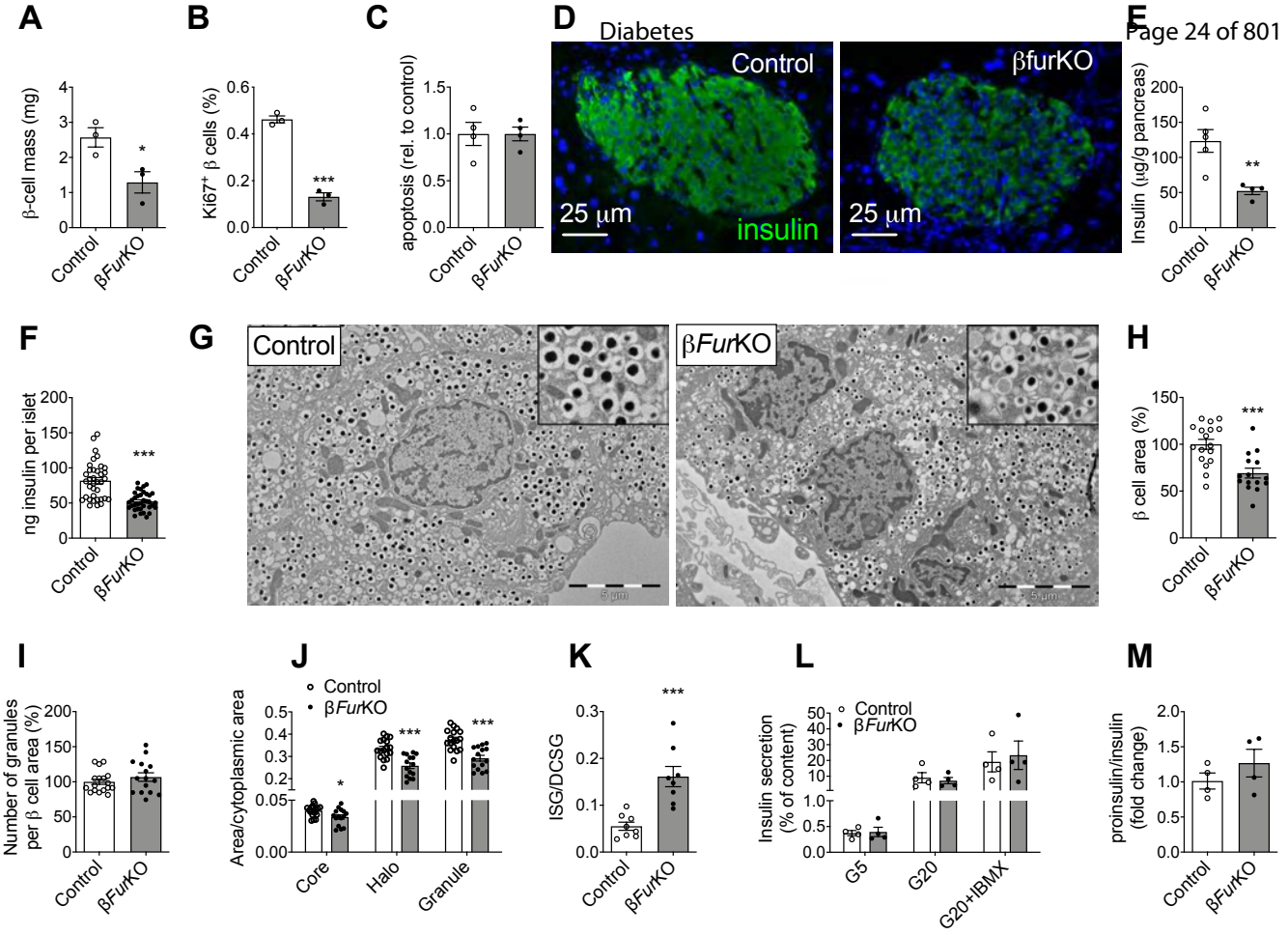
A
β-cell mass (mg)
Control
βFurKO
B
Ki67+ β cells (%)
C
apoptosis (rel. to control)
D
Diabetes
Control
βfurKO
25 μm
insulin
E
Insulin (μg/g pancreas)
F
ng insulin per islet
G
Control
βFurKO
H
β cell area (%)
I
Number of granules per β cell area (%)
J
Area/cytoplasmic area
Core
Halo
Granule
K
ISG/DCSG
L
Insulin secretion (% of content)
G5
G20
G20+IBMX
M
proinsulin/insulin (fold change)

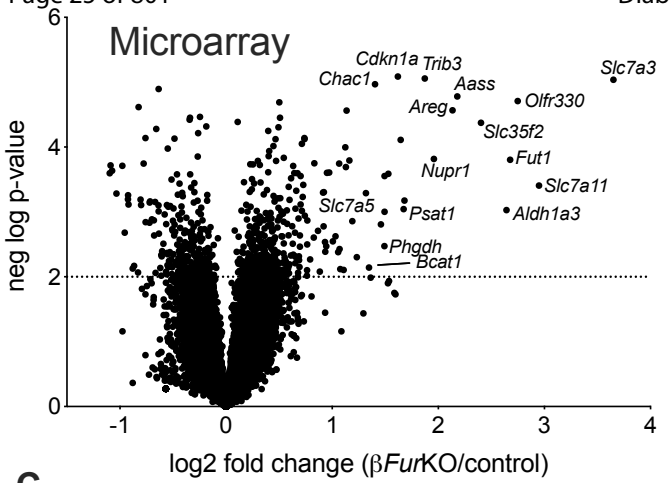

B

Ingenuity Pathway Analysis
ATF4; p=2.86E-30

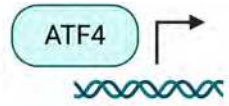

AA transporters	AA metabolism	aminoacyl-tRNA synthetases	Stress related genes
Slc1a4	*Aass*	*Eprs*	*Atf5*
Slc1a5	*Asns*	*Mars1*	*Chop [=Ddit3]*
Slc35f2	*Bcat1*		*Cdkn1a*
Slc6a9	*Cth*		*Eif4ebp1*
Slc7a3	*Gpt2*		*Fam129a*
Slc7a5	*Phgdh*		*Nupr1*
Slc7a11			*Sel1l*
			Trib3
			Stard5

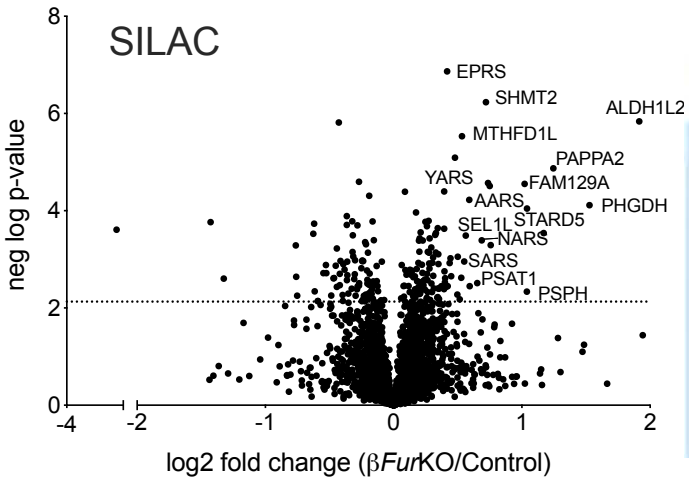

D

Ingenuity Pathway Analysis
ATF4; p=3.59E-30

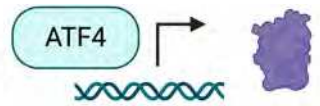

AA transporters	AA metabolism	aminoacyl-tRNA synthetases	Stress related proteins
-	PCK2	AARS	ALDH1L2
	PHGDH	CARS	FAM129A
	PSAT1	EPRS	SEL1L
	PSPH	IARS	STARD5
	SHMT2	NARS	
		LARS	
		SARS	
		TARS	
		YARS	

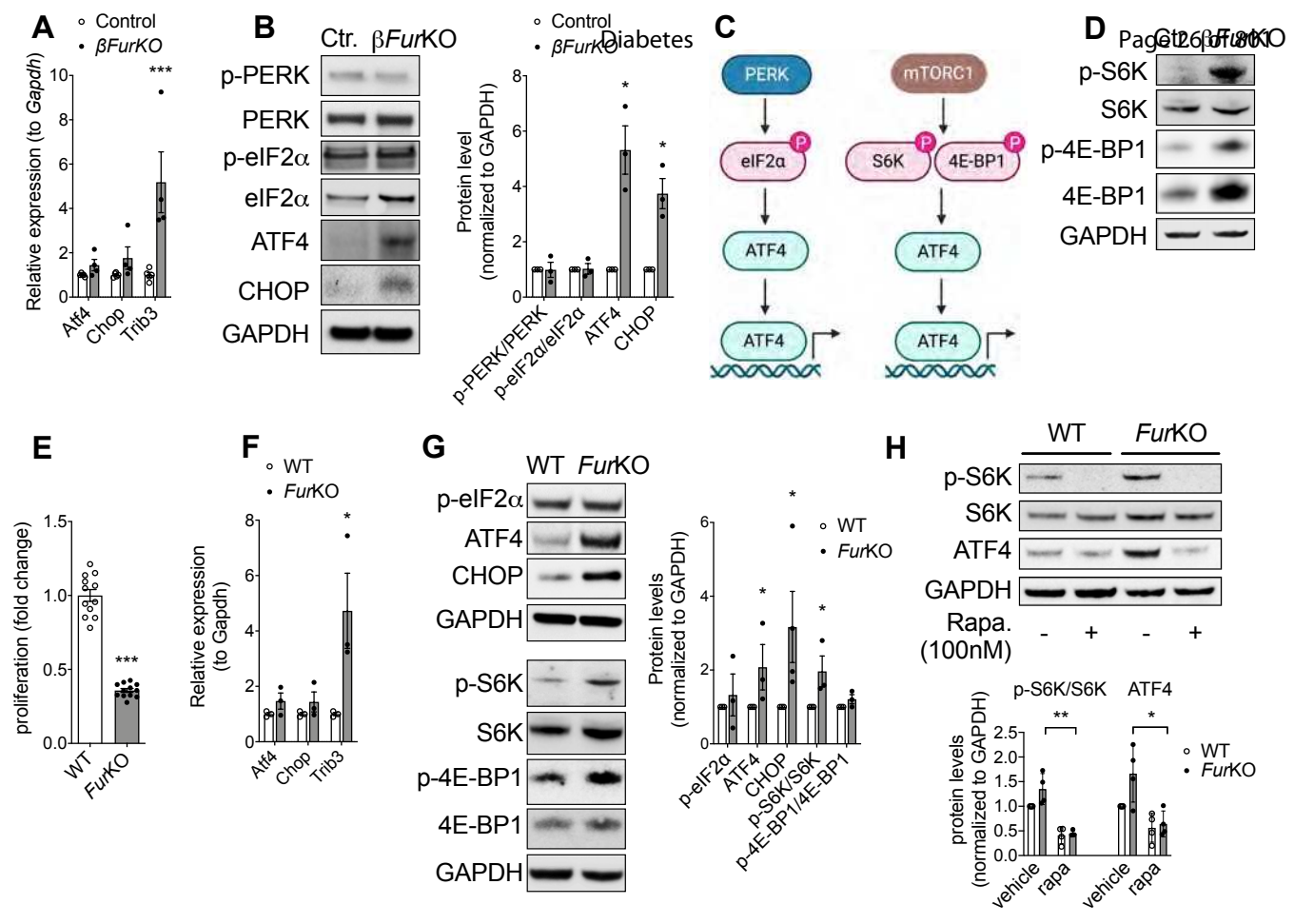
A
Control
βFurKO
Relative expression (to Gapdh)
Atf4
Chop
Trib3
B
Ctr.
βFurKO
p-PERK
PERK
p-eIF2α
eIF2α
ATF4
CHOP
GAPDH
Control
βFurKO
Diabetes
Protein level (normalized to GAPDH)
p-PERK/PERK
p-eIF2α/eIF2α
ATF4
CHOP
C
PERK
eIF2α
ATF4
ATF4
mTORC1
S6K
4E-BP1
ATF4
ATF4
D
Ctr.
βFurKO
p-S6K
S6K
p-4E-BP1
4E-BP1
GAPDH
E
proliferation (fold change)
WT
FurKO
F
WT
FurKO
Relative expression (to Gapdh)
Atf4
Chop
Trib3
G
WT
FurKO
p-eIF2α
ATF4
CHOP
GAPDH
p-S6K
S6K
p-4E-BP1
4E-BP1
GAPDH
Protein levels (normalized to GAPDH)
WT
FurKO
p-eIF2α
ATF4
CHOP
p-S6K/S6K
p-4E-BP1/4E-BP1
H
WT
FurKO
p-S6K
S6K
ATF4
GAPDH
Rapa. (100nM)
- + - +
p-S6K/S6K
ATF4
protein levels (normalized to GAPDH)
vehicle
rapa
vehicle
rapa
WT
FurKO

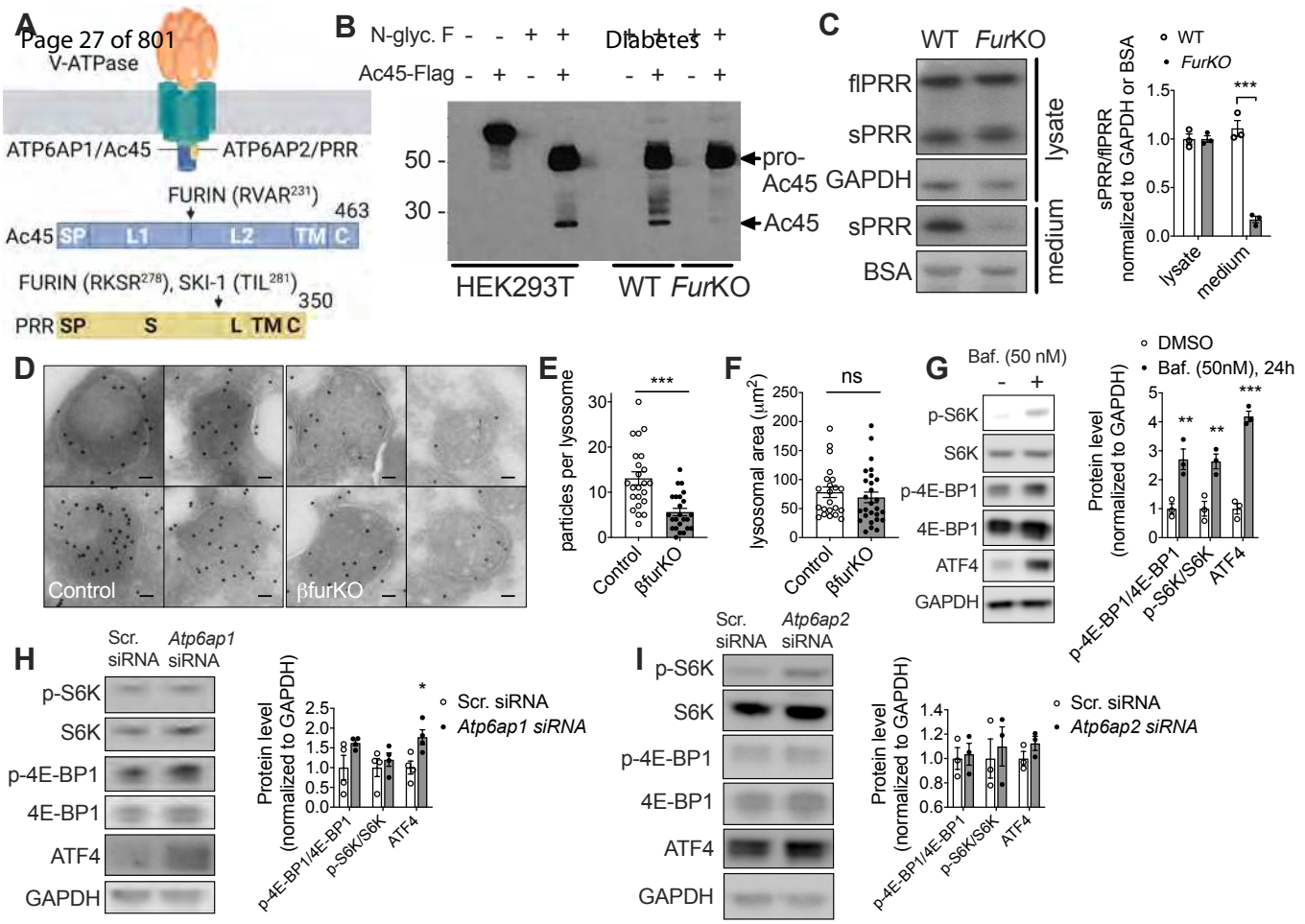
A
V-ATPase
ATP6AP1/Ac45
ATP6AP2/PRR
FURIN (RVAR231)
463
Ac45 SP L1 L2 TM C
FURIN (RKSR278), SKI-1 (TIL281)
350
PRR SP S L TM C
B
N-glyc. F - - + +
Ac45-Flag - + - +
50 -
30 -
pro-Ac45
Ac45
HEK293T
WT FurKO
Diabetes
C
WT FurKO
flPRR
sPRR
GAPDH
sPRR
BSA
lysate
medium
WT
FurKO
sPRR/flPRR normalized to GAPDH or BSA
lysate
medium
D
Control
βfurKO
E
particles per lysosome
Control
βfurKO
F
lysosomal area (μm2)
ns
Control
βfurKO
G
Baf. (50 nM)
p-S6K
S6K
p-4E-BP1
4E-BP1
ATF4
GAPDH
DMSO
Baf. (50nM), 24h
Protein level (normalized to GAPDH)
p-4E-BP1/4E-BP1
p-S6K/S6K
ATF4
H
Scr. siRNA
Atp6ap1 siRNA
p-S6K
S6K
p-4E-BP1
4E-BP1
ATF4
GAPDH
Protein level (normalized to GAPDH)
Scr. siRNA
Atp6ap1 siRNA
p-4E-BP1/4E-BP1
p-S6K/S6K
ATF4
I
Scr. siRNA
Atp6ap2 siRNA
p-S6K
S6K
p-4E-BP1
4E-BP1
ATF4
GAPDH
Protein level (normalized to GAPDH)
Scr. siRNA
Atp6ap2 siRNA
p-4E-BP1/4E-BP1
p-S6K/S6K
ATF4

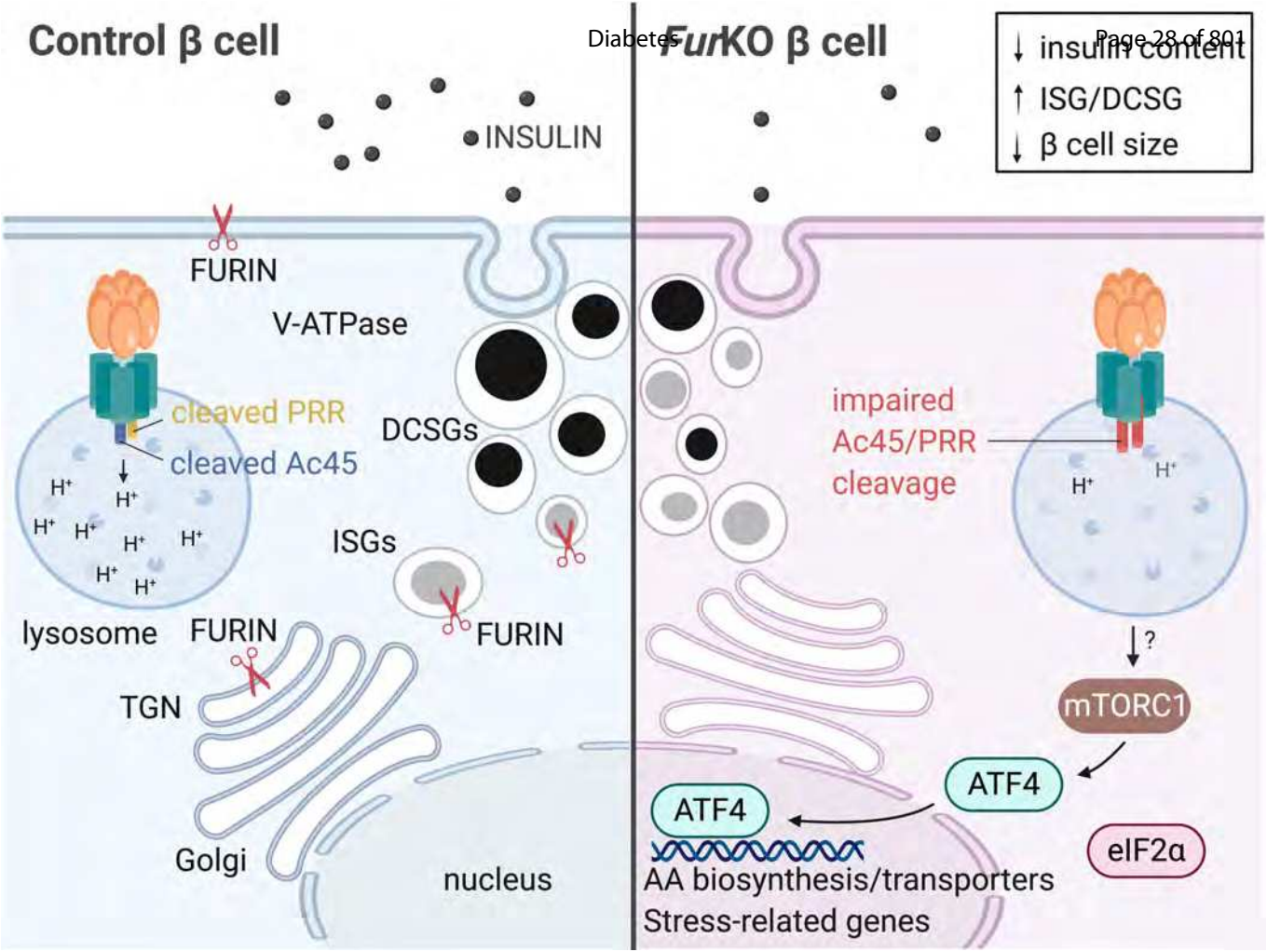
Control β cell
FurKO β cell
↓ insulin content
↑ ISG/DCSG
↓ β cell size
INSULIN
FURIN
V-ATPase
cleaved PRR
cleaved Ac45
DCSGs
ISGs
lysosome
FURIN
FURIN
TGN
Golgi
nucleus
impaired
Ac45/PRR
cleavage
?
mTORC1
ATF4
ATF4
eIF2α
AA biosynthesis/transporters
Stress-related genes

Supplemental Figures and Tables

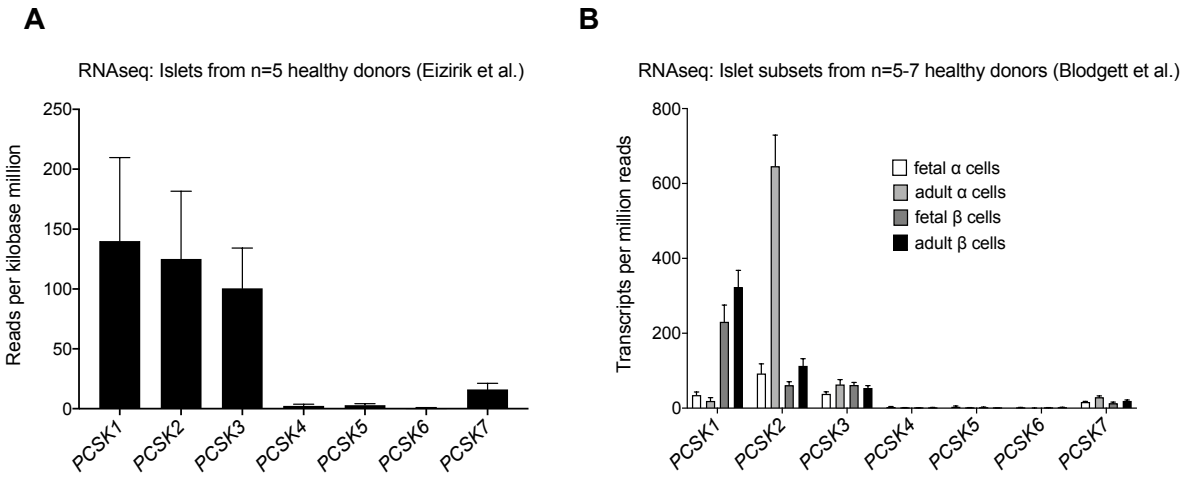

Figure S1 (A) RNA sequencing data of islets from healthy human donors (n=5) (taken from (1)). Data are shown as reads per kilobase million. (B) RNA sequencing data from islet subsets (i.e. fetal or adult α or β cells) from 5-7 healthy donors (taken from (2)). **Related to Figure 1.**

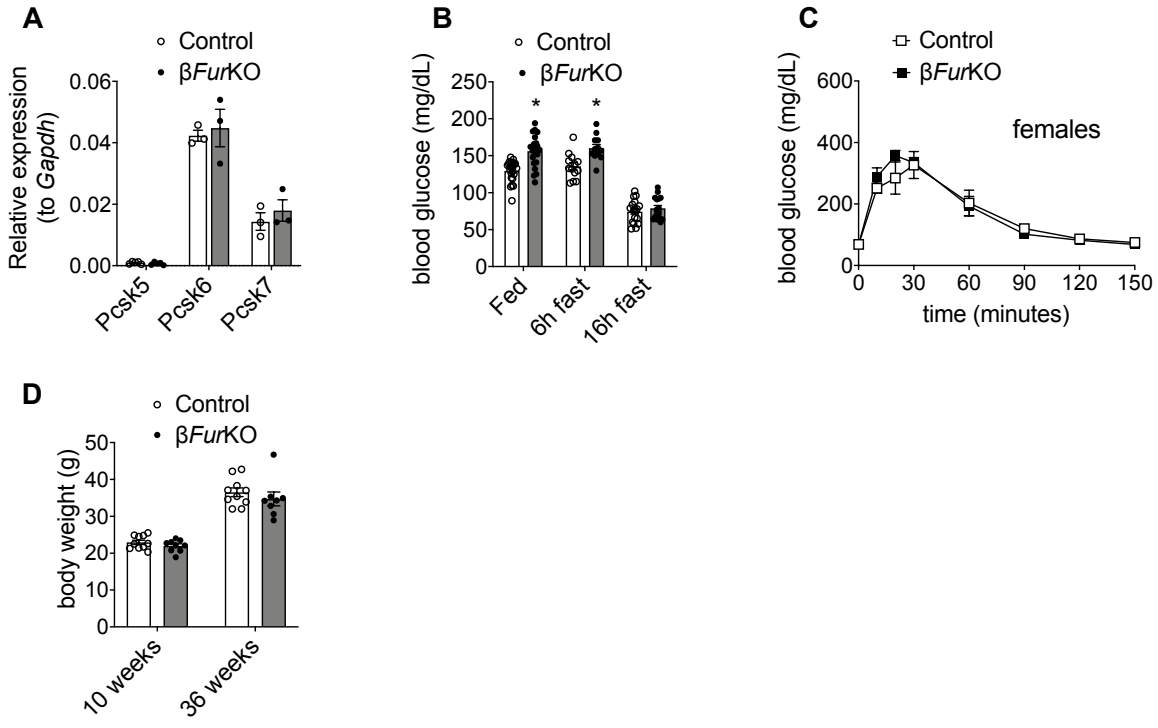

Figure S2 (A) qRT-PCR analysis of islet *Pcsk5, Pcsk6*, and *Pcsk7* mRNA from 12-week-old β*Fur*KO and control mice, n=3-5 per group, **P<0.01. (B) Blood glucose levels measured in 10-week-old

β*Fur*KO and control mice, in a random fed state, and after a 6h or an overnight (ON, ~16h) fast, n=12-23 animals per group, *P<0.05. (C) IPGTT on 10-week-old female mice, (n=4)/genotype. (D) Body weight (g) of 10-week-old and 36-week-old male control and β*Fur*KO mice (n=9-10/group). **Related to Figure 2.**

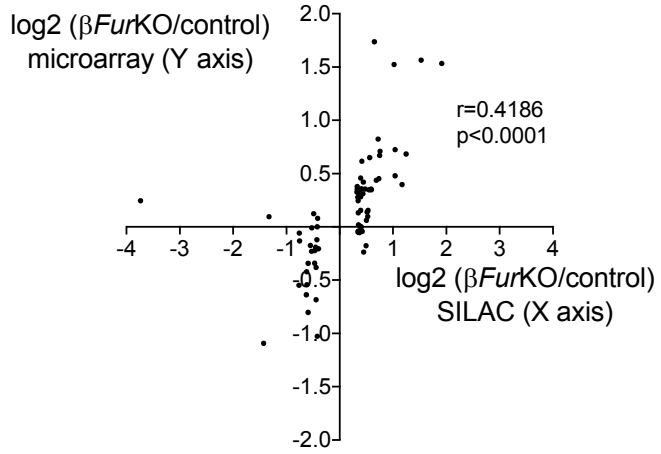

Figure S3 Correlation between SILAC and microarray data (r=0.4186, p<0.0001), for proteins that show at least a 25% increase or decrease in expression as quantified in the SILAC experiment. **Related to Figure 4.**

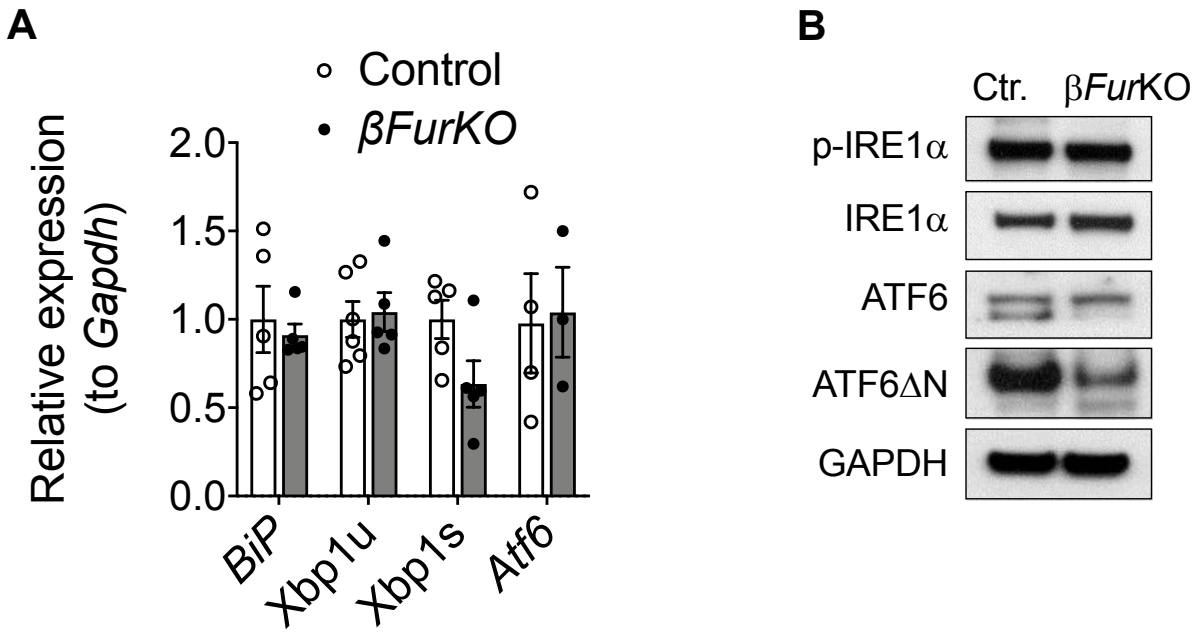

Figure S4 (A) qRT-PCR expression of genes involved in the unfolded protein response (UPR): binding immunoglobulin protein (*BiP*), unspliced and spliced X-box binding protein 1 (*Xbp1u*, *Xbp1s*) and Activating transcription factor 6 (*Atf6*), n=3-6 per group. (B) Protein analysis of total and phosphorylated Inositol-requiring protein 1 (IRE1α), and uncleaved and cleaved activating transcription factor 6 (ATF6, ATF6ΔN). GAPDH was used as a loading control. **Related to Figure 5.**

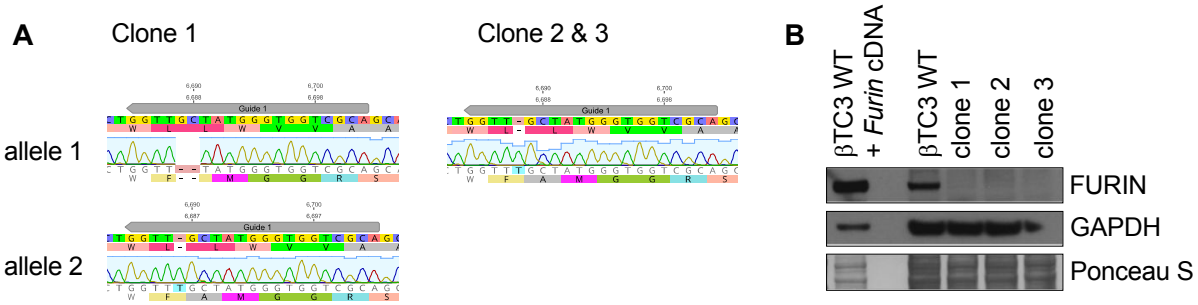

Figure S5 (A) Position of the CRISPR guide (gray) in mouse exon 2 of the *Pcsk3* gene, and the indels in the 3 different βTC3 clones. The first clone is compound heterozygous and contains a 2-bp deletion in the first allele (GC), and a 1-bp insertion in the second allele (T), leading to a frameshift on both alleles. In clones 2 and 3 we observed a 1-bp insertion (T) in all alleles tested, suggesting a homozygous mutation leading to a frameshift. (B) Protein immunoblotting of cell extracts from control and furin knockout βTC3 cells engineered using CRISPR Cas9 editing. GAPDH and Ponceau S staining were used as loading control. **Related to Figure 5.**

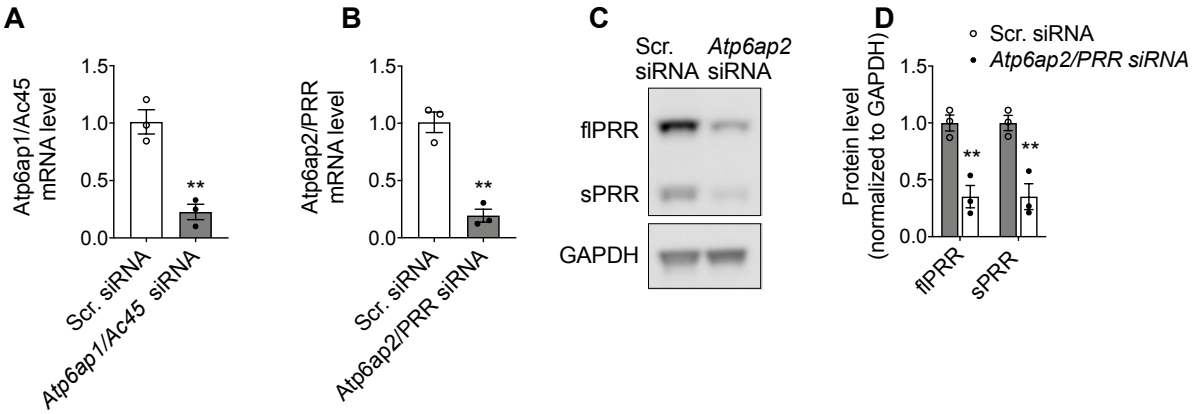

Figure S6 (A) Knockdown efficiency of *Atp6ap1/Ac45* in βTC3 cells measured by qRT-PCR, n=3 independent experiments. (B) Knockdown efficiency of *Atp6ap2/Prr* in βTC3 cells measured by qRT-PCR (B) and western blot (C), including western blot quantification (D), n=3 independent experiments. For western blot, GAPDH was used as a loading control. **P<0.01 determined by unpaired t-test. **Related to Figure 6.**

Table S1 Differentially expressed genes found by microarray, p<0.01, |fold change| ≥ 1.5.

Table S2 Ingenuity enrichment analysis for disease and functions, based on the microarray dataset.

Table S3 Ingenuity upstream regulator analysis, based on the microarray dataset.

Table S4 Proteins identified by SILAC. The highlighted proteins (gray) meet the p<0.0072 criteria.

Table S5 Ingenuity enrichment analysis for disease and functions, based on the SILAC dataset.

Table S6 Ingenuity canonical pathway analysis, based on the SILAC dataset.

Table S7 Ingenuity upstream regulator analysis, based on the SILAC dataset.

Table S8 General information on human islet donors used for qRT-PCR in Figure 1.

Table S9 Human and mouse primers used for qRT-PCR (listed in 5' - 3' direction), genotyping and CRISPR-Cas9 gene editing.

Supplemental Material

Intraperitoneal glucose (IPGTT), insulin (IPITT) tolerance tests and glucose stimulated insulin secretion (GSIS)

Male WT, Flox, Cre, Het and β*Fur*KO mice fed a normal chow diet were fasted overnight and injected with 2 mg/g body weight (BW) D-glucose (IPGTT) or 0.75 IU/g BW human insulin (ITT) in PBS, respectively. Blood glucose levels were monitored at indicated time-points using a Contour Glucometer (Roche). Mice were analyzed at ages 10 weeks, 20 weeks and 36 weeks as indicated. In a separate experiment, to establish secreted insulin levels, 24-week-old mice were fasted overnight and injected with a single intraperitoneal bolus of 3 mg/g D-glucose dissolved in PBS. Subsequently, plasma samples

were collected at indicated time points and analyzed for insulin using the Ultrasensitive Mouse Insulin ELISA (Mercodia).

Immunofluorescence of Dissociated Human Islets

Human pancreatic islets were obtained from the NIDDK-funded Integrated Islets Distribution Program (IIDP) at City of Hope. Dispersed human islet cells were stained as previously described (3). Briefly, human islets from 2 donors (1 healthy and 1 T2D) were dispersed to single-cell by a 6-8 min digestion with Accutase (ThermoFisher Scientific) at 37 °C with dispersal by a p1000 micropipettor every 45 seconds. Cells were seeded on chamber-slide wells (Sigma) coated with Geltrex (ThermoFisher Scientific) and cultured overnight in PIM(T)-medium (provided by IIDP) at 37°C in 5% CO2 incubator. Samples were fixed in 4% pre-warmed paraformaldehyde (PFA) for 30 min and acetone-methanol (1:3) for 3 min and then permeabilized 30 min in PBS with 0.2% Tween before being blocked with 1% Bovine Serum Albumin (BSA, Sigma) in PBS. Slides with sorted islets were immunostained with 1/500 furin antibody (ThermoFisher Scientific, PA1-062) and 1/50 insulin antibody (Dako, A0564) overnight at 4C. Secondary antibodies Alexa 488 anti-guinea pig and Cy3 anti rabbit from Jackson Immunoresearch (1/100) were added the next day and slides were mounted with ProLong Gold Antifade Mounting containing DAPI (ThermoFisher Scientific). Stained islet cells were examined with a Leica DM6 microscope and LAS X software.

Immunofluorescence (IF) on mouse pancreata

Pancreata were isolated and fixed in 4% paraformaldehyde (PFA) in PBS at 4°C overnight. Subsequently, they were dehydrated by a graded series of ethanol and butanol and embedded in paraffin. Sections were cut at 5μm thickness. Sections were deparaffinized, rehydrated and boiled for 20 minutes in Target Retrieval solution (Dako) to recover epitopes. Slides were blocked with 20% fetal calf serum (FCS) in PBS and incubated overnight with 1/10 anti-insulin (Dako) and 1/500 anti-Ki67 (Abcam) in Antibody Diluent (Dako) and subsequently incubated with Alexa antibodies (1/500) for 1h at room temperature. For Ki67 staining, six pancreatic sections per mouse, sampled every 200 μm, were stained

for insulin and Ki67, and all islets found on these sections were photographed using a Nikon C2 Eclipse confocal microscope, 20x magnification. The number of Ki67 $^{+}$ cells and the total number of β cells were counted using Image J software, and proliferation was calculated as (number of Ki67+ β cells/total number of β cells) x 100%.

β cell mass quantification

β cell mass of 24-week-old male mice was determined using a previously described protocol (4). Six pancreatic sections per mouse, sampled every 200 µm, were stained for insulin using standard IHC protocols. Briefly, sections were heated for 20 min in Target Retrieval Solution (Dako), blocked in 20% FCS and incubated with anti-insulin (1/10, Dako) in Antibody Diluent for 2h, followed by peroxidase-coupled secondary antibodies for 1h. 3'-3-Diamino-benzidine (DAB+, Dako) was used as substrate chromogen, after which sections were counterstained with hematoxylin and mounted. Six insulin-stained sections per mouse were photographed using a Zeiss Axioimager (Zeiss). Axiovision software (Micro Imaging, Heidelberg, Germany) was used to determine the relative insulin-positive area for every section. Subsequently, the β cell mass (mg) was calculated by multiplying relative insulin-positive area by the weight of the pancreas in mg.

Pancreatic insulin content

Total pancreatic insulin content was determined using the acid/ethanol extraction method. Briefly, pancreata were homogenized in acid/ethanol (0.12 M HCl in 75% ethanol) and after overnight incubation at -20°C, samples were centrifuged at 3,500 rpm for 15 min at 4°C to remove cell debris. Insulin content was determined using the Rat High Range Insulin ELISA (Mercodia).

Islet isolation

Islets were isolated by locally injecting the pancreas with 1 Wünsch unit/ml Liberase (Roche) in HANKS buffer as previously described (5). Injected pancreata were incubated for 18 min at 37°C in a shaker (220 rpm) and subsequently the islet fraction was separated from exocrine tissue using a Dextran

T70 gradient. Finally, islets were handpicked twice in HANKS buffer under a stereomicroscope to reach a pure islet fraction for further processing.

Islet Insulin Content and Release

For insulin secretion measurements, size-matched islets (n = 5 islets per tube, in triplicate for each condition per mouse) were placed in glass tubes containing HEPES Krebs solution 0.5% BSA supplemented with glucose: 5 mM (G5), 20 mM (G20), or G20 with 250 μM IBMX (Sigma). Supernatant was collected after 1 h incubation at 37ºC. The islets were sonicated for 3 min after adding acid ethanol (final concentration: 75% EtOH, 0.1 N HCl, 1% Triton). Samples were stored at 20ºC until quantification. The ELISA kit used for insulin determination was from Crystal Chem. Proinsulin levels were measured in the conditioned medium from islets incubated at 20mM glucose (samples from Figure 3L). Secreted proinsulin/insulin was normalised to total insulin content, similar to Figure 3L. The ELISA kit to quantify proinsulin was from Mercodia.

Cell culture and transfection

The mouse insulinoma cell line βTC3 was cultured in DMEM:F12 (1:1) supplemented with 10% heat inactivated fetal bovine serum, 100 U/ml penicillin, and 100 μg/ml streptomycin. For overexpression experiments, βTC3 cells were transfected with plasmids encoding mouse FURIN and/or mouse *ATP6AP1*/*AC45*-Flag using Lipofectamine 2000 (Life Technologies) according to the manufacturer's protocol. For knockdown experiments, βTC3 cells were transfected with SMARTpool siGENOME mouse *Atp6ap1/Ac45* (Dharmacon cat. #M-060210-01-0005) or *Atp6ap2/Prr* (Dharmacon cat. #M-063641-02-0005) using Lipofectamine RNAiMax (Life Technologies) according to the manufacturer's protocol. The Stealth siRNA Negative Control, siGENOME non-targeting siRNA control pools (Dharmacon cat. #D-001206-13-05) was transfected as a control. Cells were harvested 48 hours after transfection. PRR knockdown was verified by western blot, Atp6ap1/*Ac45* knockdown was confirmed by qRT-PCR.

Apoptosis assay

Apoptosis was measured in freshly isolated islets using the Cell Death ELISA kit (Roche) according to the manufacturer's protocol.

Cell proliferation assay

βTC3 cells were plated in triplicates at a density of 1×10^4 cells/well in 96-well plates and then incubated for 72 h. Cell proliferation was measured using the mitochondrial dye WST-1. Briefly, cells were incubated with 10 µl of WST-1 reagent per well for 2h, and the absorbance was measured at 450 and 600 nm. Three independent experiments were performed with the results presented ± SEM for the mean of all assays.

Electron Microscopy (EM)

Staining for the analysis of ultrastructures

Freshly isolated islets of 24-week-old male mice were washed with PBS, fixed with 4% formaldehyde/0.1% glutaraldehyde in 0.1 M sodium cacodylate buffer (pH 7.4), and pelleted at 13,000 rpm for 5 min. The fixative was aspirated, and the cell pellet was resuspended in warm 10% gelatin (sodium cacodylate buffer). The islets were then collected by centrifugation (4000 rpm for 1 min) and the gelatin-enrobed pellet was set on ice for 30 min, post-fixed in 1% osmium tetroxide for 2 h, dehydrated in increasing concentrations of ethanol, stained with 2% uranyl acetate and embedded in agar low viscosity resin.

After trimming the resin block containing the cell pellets, 70 nm sections were cut using a Reichardt Ultracut E ultramicrotome. The sections were collected as ribbons of 3-4 sections on a 75-mesh grid (Ted Pella). Every grid was then post stained with 3% uranyl acetate in water for 10 minutes and Reynold's lead citrate for 2 minutes. EM images were taken at 2500x magnification by a JEOL TEM1400 transmission electron microscope equipped with an Olympus SIS Quemesa 11 Mpxl camera at 80 kV. Random single sections from β cells (15 cells total) that possessed multiple dense-core granules and well-fixed cellular constituents (mitochondria, nuclear material and plasma membrane) were selected for the analysis. The plasma membranes, granules and nuclear borders of each β cell were manually marked in transmission electron microscopy (TEM) micrographs. Scanned images were

elaborated with the open-source software Microscopy Image Browser (MIB) to generate a mask of the cell compartments and the nucleus, and imported into ImageJ (National Institutes of Health, Bethesda, MD, USA) for image analysis. The immature secretory granules were distinguished from the mature secretory granules on the basis of the core electron-density and the presence of a distinctive, less pronounced halo as described by others (6).

Immunolabeling for the analysis of lysosomal pH (Tokuyasu method)

The islets of 20 week-old male mice were isolated as previously described and pre-incubated with 30 μM of DAMP (in HANKS buffer 0.02% BSA) at 37°C for 1h, and subsequently washed 2 times with the same buffer (100 rpm, 30 sec), then fixed for 1 hour at room temperature with 4% formaldehyde/0.2% glutaraldehyde in 0.1 M sodium cacodylate buffer (pH 7.4), and centrifuged at 5500 rpm for 1 min. The fixative was aspirated, and after 2 washes with HANKS buffer 0.02% BSA, the islet pellet was resuspended in warm 12% gelatin (0,1M phosphate buffer). The islets were then collected by centrifugation (13000 rpm for 5 min) and the gelatin-enrobed pellet was put on ice for 30 min. The solidified gelatin pellet with the islets aligned on the bottom was cautiously detached from the base of the Eppendorf tube, cut into smaller blocks, and submerged in a 2,3 M sucrose solution for 24h. The blocks were then mounted on cryo pins (#BS4620, Sapphire products limited, UK) and snap-frozen in liquid nitrogen. Ultrathin cryosections (70 nm thick) were cut using a Leica Ultracut UC7 with Leica FC7 cryo chamber and collected on glow discharged carbon-coated copper 200-mesh grids (#1800-F, Van Loenen Instruments, The Netherlands) with a 1:1 mixture of 2,3 M sucrose and 2% methylcellulose solution.

After floating on 2% gelatin in PBS at 37°C, grids were blocked with 0,15% glycine in PBS (3 times, 2 min each), 2% BSA in PBS for 15 minutes, and 0,1% BSA-c (#900099, Aurion, The Netherlands) in PBS (3 times, 2 min each). After blocking, grids were incubated with rabbit anti-DNP (1:400) in PBS 0,1% BSA-c for 1 hour. The primary antibody was detected with 15 nm gold protein A (#815.111,

Aurion, The Netherlands). The labeling was stabilized with 2% glutaraldehyde in PBS and washed with Milli Q water 6 times, 2 minutes each.

The lysosomes were imaged in a JEOL JEM1400-LaB6 Transmission Electron Microscope (TEM) equipped with an Olympus Quemesa 11Mpx camera at 25000x magnification. The gold particles of each lysosome were manually counted, and the lysosomal area was measured by using the Imagej software. The identification of the lysosomal ultrastructures was determined by the help of a few sections separately stained with the lysosomal marker LAMP-1 1/50 DSHB (Developmental Studies Hybridoma Bank), 1D4B, and then detected with a goat anti rabbit 6nm 1/30 (data not shown).

Western blot

Freshly isolated islets from 12 to 20 week-old male mice were lysed in Lysis buffer (Cell Signaling Technology) supplemented with protease and phosphatase inhibitor cocktails (Roche) by sonication on ice. βTC3 or HEK293T cells were lysed in 1x Ripa and extraction lysis buffer (Thermo Scientific) respectively, supplemented as above. Protein concentration was determined by BCA analysis (Thermo Scientific). Samples were boiled for 10 minutes in 4% β-Mercaptoethanol and 1x sample buffer (Thermo Scientific) and loaded on a 10% Bis/Tris gel with MES or MOPS running buffer for SDS-PAGE analysis. Proteins were transferred to a nitrocellulose blot, blocked with a blocking buffer (5% non-fat milk, 0.2% Triton X-100 in PBS) and subsequently incubated with primary antibody in the blocking buffer at 4°C overnight. Blots were washed in PBS 0.2% Triton X-100, incubated with peroxidase-conjugated secondary antibody (Dako) for 1h, and proteins were detected using the Western Lightning ECL System (PerkinElmer). For deglycosylation experiments, 100 µg of proteins from the cell lysate were boiled at 95°C for 5 min in sodium phosphate buffer 0.1% SDS and □-Mercaptoethanol (diluted 1:6 in water) in a total volume of 35ul. Once cooled down, the samples were supplemented with 0.8% NP-40 and 1 Unit of N-glycosidase F (Roche) in a final volume 50ul and incubated at 37°C overnight. The samples were then processed for western blot as above. The primary antibodies used were rabbit anti-ATF4, anti-phospho-p70S6K (Thr389), anti-p70S6K, anti-phospho-PERK (Thr980), anti-PERK, anti-phospho-4E-BP1 (Thr37/46), anti-4E-BP1, and anti-GAPDH from Cell Signaling

Technology; mouse anti-CHOP and, anti-eIF2α from Cell Signaling Technology; rabbit anti-phospho-IRE1α (Ser724) and anti-Renin R from Novus Biologicals; mouse anti-flag M2 from Sigma; mouse anti-ATF6 from Novus Biologicals; mouse anti-FURIN and rabbit anti-phospho-eIF2α (Ser51) were generated as previously described (7). To determine secreted sPRR levels in the culture medium, proteins were precipitated with methanol. Briefly, βTC3 cells were plated in 6-well plates at 80% confluence, washed and incubated overnight at 37°C and 5% CO2 in 1ml of serum-free DMEM:F12 medium. Sixteen hours after incubation the conditioned medium was transferred to ice cold tubes and centrifuged at 1000 rpm at 4°C for 10 minutes. Then, an equal amount (12.5µg) of bovine serum albumin (BSA) was added to each supernatant. After the addition of BSA, the samples were vigorously vortexed and 4 ml of cold methanol was added and mixed by hand shaking. After a 2 hour at -20°C, the samples were centrifuged at 1500 rpm at 4°C for 15 minutes. Then, the supernatants were removed and the pellets were dried for 2 hours. Dried pellets were dissolved in 25 µl of 2x sample buffer and analyzed by Western blot as described above.

Stable Isotope Labeling by Amino acids in Cell culture (SILAC)

Spike-in SILAC analysis was performed to compare relative abundance of proteins in islets from 12 week-old male Flox and β*Fur*KO mice, following established protocols. To prepare the spike-in standard, MIN6 cells were cultured for 12 passages in SILAC medium Dulbecco's modified Eagle medium (DMEM), high glucose (4,5 g/l) without L-glutamine, arginine and lysine (Silantes Basic Products cat. #280001300), supplemented with 15% fetal bovine serum (FBS), glutamine PS, heavy arginine (+10) and heavy lysine (+8) (Silantes Basic Products cat. no. 282986444). Light and heavy labeled cells were lysed in freshly prepared SDT-lysis buffer (2% SDS, 50 mM DTT, 100 mM Tris HCl pH 7.6), DNA was sheared by sonication, the sample was incubated at 95°C for 5' and centrifuged. To verify the labeling efficiency, 25 µg of the cell lysate of the light labeled cells (L) were mixed with equal amounts of heavy labeled cells (H) and digested with trypsin using the FASP protocol. After analysis of the sample on a Q Exactive mass spectrometer (Thermo Scientific), more than 99% of the peptides had a $\log_2$ normalized ratio between -1 and 1, demonstrating efficient labeling.

Sample preparation for proteomic analysis

Islets from 4 WT and 4 β*Fur*KO mice were isolated as previously described and were pooled per 2 mice of the same genotype to obtain at least 20 µg of proteins upon lysis in SDT-lysis buffer. Twenty µg of islet lysate was pooled with equal amounts of the spike-in standard and digested with trypsin using the FASP protocol (8). Using strong anion exchange (SAX) on a StageTip format (Thermo Scientific), 3 fractions (pH 3, 6 and 11) were obtained and analyzed on a Q Exactive mass spectrometer. The quality of the spike-in standard was analyzed as described before. For more than 90% of the proteins the difference in experimental sample and the standard was <5, suggesting that the spike-in standard was of good quality.

Mass spectrometry

Samples were analyzed by LC-MS/MS, coupling an Easy nLC1000 nanoflow HPLC system to the Q Exactive benchtop mass spectrometer (both Thermo Fisher Scientific) as described previously (9). Data were analyzed using the MaxQuant software environment (version 1.3.0.5) as previously described. Statistical evaluation of the data was performed with the freely available Perseus statistics software (version 1.2.0.7) and Microsoft Excel. Common contaminants and reverse decoy matches were removed from the protein identification list. At least 2 unique peptides per protein were required for protein identification. H/L ratios were reversed to L/H ratios. Only proteins that were identified and quantifiable in at least three biological replicates in each group were used for relative quantification. The average group means of the ratios were calculated and data are expressed as the log2 value of the ratio of ratios (β*Fur*KO/control). For statistical evaluation, a two-sided t-test was used. The p-value was corrected using false discovery rate (FDR) based multiple hypothesis testing. Both t-test and FDR based multiple hypothesis testing were carried out with the default settings of the Perseus statistics software.

Quantitative RT-PCR (qRT-PCR)

RNA from mouse islets or βTC3 cells was isolated using the Nucleospin RNA II (Macherey Nagel) kit according to the manufacturer's protocol. cDNA was synthetized using the iScript cDNA synthesis kit (Bio-Rad). Primers were designed using the ProbeFinder software (Roche Applied Sciences). qRT-PCR

was performed in triplicate with a MyiQ single-color real-time PCR detection system (Bio-Rad) using SYBR Green. RNA from human islets (~150 for each donor) was extracted with RNeasy Mini Kit (Qiagen) and was reverse transcribed using the High Capacity Reverse Transcription Kit (Applied Biosystems). qRT-PCR was performed with a ViiA 7 detection system from Life Technologies (Thermo Fisher Scientific) using SYBR Green PCR master mix (Bioline). Data is represented as 2ˆ-ΔCt compared to average of PC1/3 in healthy group. Primers for human and mouse genes are listed in **Table S9**.

Statistical analysis

Results are expressed as means ± SEM. Statistical analysis was performed by unpaired Student's t test or two-way ANOVA with post-hoc Bonferroni correction for pairwise time-specific differences between genotypes. GraphPad Prism 8 software was used for all analyses. A value of $p<0.05$ was considered significant.

Supplemental references

1. Eizirik DL, Sammeth M, Bouckenooghe T, Bottu G, Sisino G, Igoillo-Esteve M, et al. The human pancreatic islet transcriptome: expression of candidate genes for type 1 diabetes and the impact of pro-inflammatory cytokines. PLoS Genet. 2012 Mar 8;8(3):e1002552.

2. Blodgett DM, Nowosielska A, Afik S, Pechhold S, Cura AJ, Kennedy NJ, et al. Novel Observations From Next-Generation RNA Sequencing of Highly Purified Human Adult and Fetal Islet Cell Subsets. Diabetes. 2015 Sep;64(9):3172–81.

3. Furuyama K, Chera S, van Gurp L, Oropeza D, Ghila L, Damond N, et al. Diabetes relief in mice by glucose-sensing insulin-secreting human α-cells. Nature. 2019 Mar;567(7746):43–8.

4. Brouwers B, de Faudeur G, Osipovich AB, Goyvaerts L, Lemaire K, Boesmans L, et al. Impaired islet function in commonly used transgenic mouse lines due to human growth hormone minigene expression. Cell Metab. 2014 Dec 2;20(6):979–90.

5. Gysemans CA, Waer M, Valckx D, Laureys JM, Mihkalsky D, Bouillon R, et al. Early graft failure of xenogeneic islets in NOD mice is accompanied by high levels of interleukin-1 and low levels of transforming growth factor-beta mRNA in the grafts. Diabetes. 2000 Dec;49(12):1992–7.

6. Masini M, Marselli L, Bugliani M, Martino L, Masiello P, Marchetti P, et al. Ultrastructural morphometric analysis of insulin secretory granules in human type 2 diabetes. Acta Diabetol. 2012 Dec;49 Suppl 1:S247–52.

7. Scheuner D, Vander Mierde D, Song B, Flamez D, Creemers JWM, Tsukamoto K, et al. Control of mRNA translation preserves endoplasmic reticulum function in beta cells and maintains glucose homeostasis. Nat Med. 2005 Jul;11(7):757–64.

8. Geiger T, Wisniewski JR, Cox J, Zanivan S, Kruger M, Ishihama Y, et al. Use of stable isotope labeling by amino acids in cell culture as a spike-in standard in quantitative proteomics. Nat Protoc. 2011 Feb;6(2):147–57.

9. Dislich B, Wohlrab F, Bachhuber T, Müller SA, Kuhn P-H, Hogl S, et al. Label-free Quantitative Proteomics of Mouse Cerebrospinal Fluid Detects β-Site APP Cleaving Enzyme (BACE1) Protease Substrates In Vivo. Mol Cell Proteomics. 2015 Oct;14(10):2550–63.